minerals

MDPI

Article

A Mosaic of Colors: Investigating Production Technologies of Roman Glass Tesserae from Northeastern Italy

Sarah Maltoni [1] and Alberta Silvestri [2,3,*]

[1] Department of Cultural Heritage, University of Padova, Piazza Capitaniato 7, 35139 Padova, Italy; sarah.maltoni@gmail.com
[2] Department of Geosciences, University of Padova, via Giovanni Gradenigo 6, 35131 Padova, Italy
[3] CNR-ICMATE, Corso Stati Uniti 4, 35126 Padova, Italy
* Correspondence: alberta.silvestri@unipd.it; Tel.: +39-(0)49-827-9142

Received: 25 May 2018; Accepted: 12 June 2018; Published: 16 June 2018

Abstract: In the current study, a set of 60 glass tesserae from two disrupted Roman mosaics located in Pordenone and Trento (northeastern Italy) are analyzed, with the aim of investigating the coloring and opacification techniques, with a focus on the causes of specific textural features. All the available colors and textures were selected for archaeometric analyses, in order to guarantee the full characterization of both assemblages and comparisons between the two sites. The applied analytical protocol comprises micro-textural and preliminary chemical characterizations of the tesserae by means of OM and SEM-EDS, mineralogical analysis of the opacifiers by XRD and chemical analysis of the glassy matrices by EPMA; in addition, on specific tesserae, micro-Raman spectroscopy, FORS, and EPR were also performed to clarify the type of opacifer, coloring ion and oxidation state, respectively. Results show that both the base-glass and the coloring/opacification techniques identified are consistent with the presumed Roman dating of the mosaics. All the tesserae are natron-based and chemically comparable with major Roman compositional groups, except for red samples. Antimony-based opacifiers are identified in most of the blue, turquoise, white, yellow and green tesserae, and copper-based opacifiers in the red ones; cobalt and copper are the most frequent ionic colorants used to obtain various shades of blue, turquoise and green colors. Despite the general comparability of both assemblages with the published data on glass tesserae coeval in age, the present study shows differences in the technological solutions used for obtaining the same color, and less common coloring and opacification techniques in three samples from Pordenone. The banded textures of some tesserae were also carefully investigated, and multiple factors influencing the changes in color (different distribution or relative abundance of opacifiers, crystal size, micro-texture, chemical composition of glassy matrix) are identified.

Keywords: Roman glass tesserae; micro-texture; coloring; opacification; Italy; SEM; XRD; EPMA; production technology; archaeometry

1. Introduction

Glass mosaic tesserae, like the other types of opaque colored glass, are heterogeneous materials, composed of glassy matrix and crystalline phases, and produced from selected raw materials (generally minerals) with various functions (formers, fluxes, stabilizers, colorants, decolorants and opacifiers), by means of pyrotechnological processes. In particular, color is the most important parameter characterizing glass mosaics; the special beauty of a glass mosaic partly depends on how the material is cut and shaped, but more importantly on how the various colors are first obtained and then applied

near each other in order to create an image. The glass color is determined by a combination of chemical and micro-structural effects. It is mainly due to transition metal ions (e.g., Fe^{2+}/Fe^{3+}, Co^{2+}, Cu^{2+}, and Mn^{3+}), which cause selective absorption of electromagnetic radiation in the visible band and act as coloring agents. Other coloring effects can be produced when a metal is dispersed as minute particles in the glass, the color depending on the size of the colloidal dispersion. Lastly, color may be due to crystalline phases dispersed in the matrix, which also act as glass opacifiers, due to diffusion of incident radiation, generated by refraction between the glass matrix and microcrystalline areas within the glass itself [1].

The scientific analysis so far conducted on Roman and Byzantine glass mosaic tesserae (e.g., [2–13] and references therein) highlights a significant continuity, with some major changes mostly in the opacifiers. The most common opacifiers of the Roman glassmaking are indeed antimony-based (Ca-antimonate and Pb-antimonate) and copper-based crystalline phases (cuprite and metallic copper), although they were used for a very long time (from around 1500 BC until modern times) [14–17]. Two methods of production are hypothesized for Ca-antimonate: the "corpo" method, in which the pigment is synthesized *ex situ*, and the *in situ* precipitation that is obtained by adding excess antimony to the molten glass [18]: both methods are attested in Roman and Byzantine production, with a prevalence of the *in situ* crystallization [19]. In regard to Pb-antimonate, it is commonly accepted that this compound was synthesized *ex situ* and then added to the molten glass in a very quick process [17,20]. Copper-based phases (cuprite and metallic copper), which are responsible for the orange/red color and opacity of the glass, are always synthesized *in situ*, if reducing conditions are established in furnaces, and previous studies have been demonstrated that lead and copper play an important role in influencing the type of synthesized phase, and, that texture, size and abundance of crystals may influence hue [15,21,22]. After the 4th century AD the antimony-based opacifiers are progressively substituted by tin compounds (e.g., cassiterite and Pb-stannate), bone ash, and ground quartz, as testified by the Byzantine and medieval mosaics so far analyzed (e.g., [5,11,23,24]). Independently from the age of mosaics, the most common intentional ionic colorants are cobalt and copper for the blue and green [25] and manganese for the purple glasses [26].

Despite the great number of papers dedicated to Roman and Byzantine mosaic tesserae (e.g., [2,3,6,8,10,12,27] and references therein), relatively little attention is still given to the textural features of these artefacts, which can provide useful information on raw materials, temperatures, times of firing, and opacification techniques. In particular, banded tesserae, that are present in Roman and Byzantine mosaics, are underrepresented in the archaeometric literature and, when included, little or no attention is dedicated in investigating the causes of the non-homogenous textures and the generation of the various colors.

The present study, analyzing a selection of 60 tesserae from two disrupted Roman mosaics, characterized by a wide range of colors and textures, gives valuable insights into the high technological skills of the Roman glassmakers and in the variety of technological solutions employed in the production of each color. In addition, it aims at expanding the database on Roman glass tesserae from Italy, and the understanding of the textural characteristics of opaque colored glass, with a focus on banded tesserae, in the main perspective of color generation. Complementary analytical techniques (OM; SEM-EDS; XRD; EPMA) are here applied for textural, chemical, and mineralogical study of glassy matrix and crystalline phases in tesserae. These techniques are coupled with other spectroscopic methods (EPR, FORS and micro-Raman spectroscopy), to address specific questions related to the type of coloring ions and opacifiers used in some tesserae.

2. Materials and Methods

The glass tesserae investigated here come from two inland cities of northeastern Italy, Pordenone and Trento; both assemblages derive from disrupted mosaic decorations that were excavated in secondary sites.

The tesserae from Pordenone were excavated in the Roman villa of Torre. The first archaeological investigations were conducted between 1940 and 1952, under the guidance of the owner of the area, the Earl of Ragogna, who was an enthusiastic self-taught scholar [28]. The excavations were conducted in the absence of a stratigraphic approach and, for this reason, tesserae and mosaic fragments cannot be precisely dated. The life span of the villa is wide (1st–5th century AD), but a large quantity of glass tesserae was excavated in the baths, which were in use until 3th century AD, suggesting that an early dating may be hypothesized for the mosaic decoration [28].

The tesserae from Trento were excavated under the main church of *Santa Maria Maggiore*, and they likely come from the decoration of the pre-existing Roman bath, built in the 2nd century AD and disrupted in the 4th century AD for the construction of the paleo-Christian church. The chronological frame considered for the tesserae is 2nd to 4th century AD, but the mosaic decoration (and consequently the tesserae) are more likely dated to the period of the construction of the baths, i.e., the 2nd century AD [29].

A selection of 60 tesserae (28 from Pordenone and 32 from Trento, labelled with the prefix PN and TN, respectively) of all the available colors, degrees of diaphaneity, and textures (Table 1—Figure 1) was devoted to archaeometric analyses. The selected tesserae were preliminarily grouped by color by means of naked-eye observation, following the colorimetric subdivision, already applied for other assemblages previously studied by authors [7,13,30]. For a more objective color classification, this subdivision was also checked by measuring colorimetric coordinates of all opaque and colored tesserae by FORS. The assemblages of Pordenone and Trento comprise 21 colors, furtherly grouped into 7 color macro-groups (colorless, turquoise, blue, white, yellow, green and red) on the basis of opacifiers and/or ionic colorants/decolorizers identified (Table 1). All the above colors are comparable in both assemblages, except for the light amber tessera identified only in Pordenone and the olive-green and dark amber ones only identified in Trento. The majority of the tesserae are opaque, although some translucent (all the dark blue and olive green, 1 blue, 3 dark green, and 1 yellow-green) and transparent (all the colorless tesserae) ones are also present. In addition, while most of the samples are uniform in color, some banded samples are identified. In detail, some samples, especially those belonging to the macro-group red (but also in the turquoise, blue, yellow, and colorless macro-groups), are banded with areas of darker and brighter color or with areas showing different colors, which can be all opaque (e.g., orange and red), opaque and translucent (e.g., red and green, respectively), or translucent and transparent (e.g., purple and colorless), and, in the case of turquoise, blue and yellow tesserae, by strips of opaque glass in a translucent colored matrix (Figure 1).

Where possible, the various glass bands are analyzed separately. This was done in the case of some colorless (samples PN AU1, PN AU2 and TN AU1, composed of supporting tessera, gold foil and *cartellina*, see Section 3.2 for further details), turquoise (PN TU2), red (PN AV2, TN AV1, and TN M2) and yellow (PN GSO2) tesserae, for a total of 68 analytical samples *vs* 60 tesserae.

A combination of analytical techniques is employed here to guarantee the complete characterization of the samples, composed of glass and crystalline phases, acting as opacifiers.

Micro-textural analyses are carried out by means of optical microscopy (OM) and scanning electron microscopy (SEM) coupled with an energy-dispersive spectrometer (EDS), which also allows the qualitative and semi-quantitative chemical analyses of both the glassy matrix and inclusions.

Optical microscopy observations were conducted under stereoscopic vision on the whole tesserae with a Zeiss Stemi 2000C microscope (Carl Zeiss, Oberkochen, Germany) and under reflected and transmitted light on the polished sections with a Nikon Eclipse Me600 (Nikon Corporation, Tokyo, Japan).

The instruments employed for SEM-EDS analyses are an ESEM FEI Quanta Inspect equipped with an Oxford energy dispersive spectrometer and a FEI Quanta 200 FEG-ESEM instrument equipped with a Genesys energy-dispersive X-ray spectrometer (Thermo Fisher Scientific, Waltham, MA, USA). In both instrumentations, SEM images were taken by collecting the backscattered electron signal (BSE), operating under high-vacuum conditions (<4 Pa) with an accelerating voltage of 20–25 kV and a working distance of approximately 10 mm.

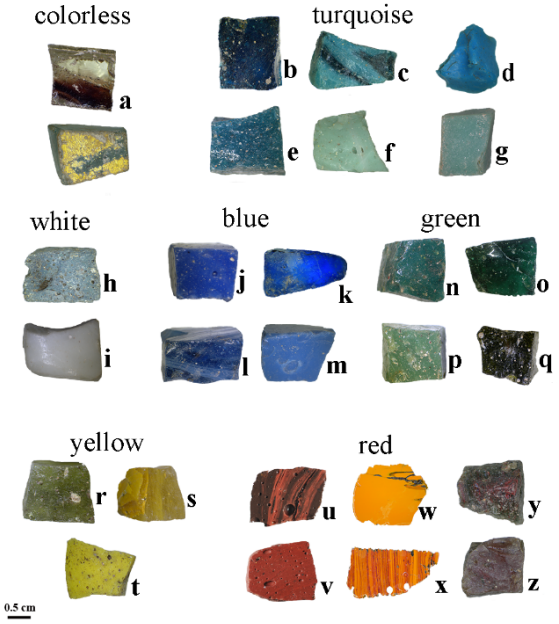

Figure 1. OM images of a selection of glass tesserae, illustrating all the colors and textures present in the assemblage investigated here: (**a**) PN AU2; (**b**) PN BS1; (**c**) PN TU2; (**d**) PN TU3; (**e**) PN AQ1; (**f**) PN CE1; (**g**) TN VCH1; (**h**) TN GR1; (**i**) PN BI OP1; (**j**) TN BO1; (**k**) TN B1; (**l**) PN AZ2; (**m**) PN AZ1; (**n**) PN VS1; (**o**) PN VTR1; (**p**) PN VP1; (**q**) TN VOL 2; (**r**) TN VG2; (**s**) PN GSO2; (**t**) TN GSO1; (**u**) TN M2; (**v**) TN M3; (**w**) PN AV1; (**x**) PN AV2; (**y**) TN VOL1; (**z**) TN NS1.

The chemical quantitative analyses of the glassy matrix are conducted, avoiding the inclusions, by means of electron microprobe (EPMA). The instrument employed is a CAMECA-SX50 (CAMECA SAS, Gennevilliers Cedex, France), equipped with four wavelength-dispersive spectrometers (WDS). The detailed EPMA analytical conditions (measured elements and lines, used analyzer crystals, current and voltage of electron beam, measure acquisition time, selected standards and detection limits) are given in Table S1. X-ray counts were converted to oxide weight percentages using the PAP (CAMECA) correction program. Precision and accuracy were checked against the international reference standard, Corning glass B [31]. Precision is within 1% for SiO_2, about 3–5% for Na_2O, CaO, and Al_2O_3, better than 10% for other elements; accuracy is lower than 1% for SiO_2, Na_2O, and FeO, lower than 5% for CaO, K_2O, P_2O_5 and Sb_2O_3 and not higher than 12% for other elements (Table S2). With EPMA, chemical compositions of glassy matrix were identified by various point microanalyses (generally 6 analytical points on the translucent and transparent tesserae and 12 points on the opaque ones) and averages and standard deviations were calculated. In order to minimize the chemical contribution of the opacifiers dispersed in the glassy matrix of tesserae (i.e., all samples, except for transparent and translucent tesserae), EPMA analyses were carried out into two steps. In a first step, Na, Mg, Al, Si, P, K, Ca, Mn and Fe were measured on about ten analytical points, randomly chosen. Since two types of opacifiers were identified, composed of antimony- or copper-based phases (see Section 3 for details), Sb, and Cu were also measured, in order to check the analysis point. In the second step, back-scattered electron images were acquired for each sample and S, Cl, Ti, Co, Ni, Cu, Zn, Sn, Sb and Pb were measured on about six analytical points, avoiding the opacifiers. Lastly, in order to match the analyses acquired during the two steps, data from Sb and Cu were used as "control elements": only first-step analyses with Sb and Cu contents comparable with those of the second step (i.e., measured values are within the precision of the method for the considered elements) were chosen, since they were considered representative only of the glassy matrix, without the contribution of the opacifiers.

Table 1. A list of glass tesserae from Pordenone (PN) and Trento (TN), subdivided by color macro-group. Colorimetric coordinates and a summary of the major textural and chemical characteristics of each tessera are also reported. (N = natron; A = soda ash; n.m.: not measured; n.a.: not attributed).

Tessera	Color Macro-Group	Color	Colorimetric Coordinates			Diaphaneity	Flux	Glassy Matrix	Opacifier	Ionic Colorant/Decoloriser
			L*	a*	b*					
PN AU1	colorless	gold		n.m.		transparent	N	Mn-glass		Mn
PN AU2	colorless	gold		n.m.		transparent	N	Mn-glass		Mn
TN AU1	colorless	gold		n.m.		transparent	N	Mn-glass		
PN AG1	colorless	colorless		n.m.		transparent	N	Mn-glass		Mn
TN TR INC 1	colorless	colorless		n.m.		transparent	N	Sb-glass		Sb
PN TU1	turquoise	turquoise	53	−21	1	opaque	N	Sb/Mn glass	Ca-antimonate	Cu
PN TU2	turquoise	turquoise	53	−20	11	translucent with opaque bands	N	Sb/Mn glass	Ca-antimonate	Cu
PN TU3	turquoise	turquoise	51	−13	−30	opaque	N	Sb-glass	Ca-antimonate	Cu
TN TU1	turquoise	turquoise	48	−19	−18	opaque	N	Mn-glass	Ca-antimonate	Cu
TN TU2	turquoise	turquoise	52	−16	−11	opaque	N	Sb/Mn glass	Ca-antimonate	Cu
TN TU3	turquoise	turquoise	60	−24	−8	opaque	N	Sb/Mn glass	Ca-antimonate	Cu
PN BS1	turquoise	dark blue	25	−1	−17	translucent	N	Sb/Mn glass		Cu
TN BS1	turquoise	dark blue	27	−1	−21	translucent	N	Sb/Mn glass		Cu
PN CE1	turquoise	pale blue	69	−18	5	opaque	N	Mn-glass	Ca-antimonate	Cu
TN CE1	turquoise	pale blue	70	−22	1	opaque	N	Sb/Mn glass	Ca-antimonate	Cu
PN AQ1	turquoise	aquamarine	52	−9	−17	semi-opaque	N	Sb/Mn glass	Quartz + bubbles + Ca-antimonate	Cu
TN AQ1	turquoise	aquamarine	49	−5	−18	opaque	N	Mn-glass	Ca-antimonate	Cu
TN AQ2	turquoise	aquamarine	54	−13	−14	opaque	N	Mn-glass	Ca-antimonate	Cu
PN VCH1	turquoise	pale green	65	−13	0	opaque	N	Mn-glass	Ca-antimonate	Cu
TN VCH1	turquoise	pale green	63	−25	4	opaque	N	Sb/Mn glass	Ca-antimonate	Cu
PN BO1	blue	blue	27	16	−62	opaque	N	Mn-glass	Ca-antimonate	Co
TN BO1	blue	blue	27	13	−45	opaque	N	Mn-glass	Ca-antimonate	Co
TN B1	blue	blue	38	21	−71	translucent	N	Mn-glass		Co
PN AZ1	blue	azure	42	4	−31	opaque	N	Mn-glass	Ca-antimonate	Co
PN AZ2	blue	azure	48	0	−26	translucent with opaque bands	N	Mn-glass	Ca-antimonate	Co
TN AZ1	blue	azure	65	−3	−13	opaque	N	Mn-glass	Ca-antimonate	Co
TN AZ2	blue	azure	53	−1	−42	opaque	N	Mn-glass	Ca-antimonate	Co
PN BIOP1	white	white	83	2	−6	opaque	N	Mn-glass	Ca-antimonates	
TN BIOP1	white	white	87	−1	−2	opaque	N	Mn-glass	Ca-antimonates	
PN GR1	white	grey	46	2	−4	opaque	N	Sb/Mn glass	Ca-antimonates	Co
TN GR1	white	grey	62	1	−3	opaque	N	Sb/Mn glass	Ca-antimonates	Co
TN GR2	white	grey	66	−6	−2	opaque	N	Mn-glass	Ca-antimonates	Co
PN GSO1	yellow	yellow	75	1	63	opaque	N	Sb/Mn glass	Pb-antimonate	

Table 1. *Cont.*

Tessera	Color Macro-Group	Color	Colorimetric Coordinates			Diaphaneity	Flux	Glassy Matrix	Opacifier	Ionic Colorant/Decoloriser
			L*	a*	b*					
PN GSO2	yellow	yellow	71	7	60	translucent with opaque bands	N	Mn-glass	Pb-antimonate	
TN GSO1	yellow	yellow	81	−7	76	opaque	N	Sb/Mn glass	Pb-antimonate	
TN GSO2	yellow	yellow	79	−6	76	opaque	N	Sb/Mn glass	Pb-antimonate	
PN VG1	yellow	yellow green	69	−12	43	opaque	N	Sb/Mn glass	Pb-antimonate	
TN VG1	yellow	yellow green	56	−2	39	semi-opaque	N	Sb/Mn glass	Pb-antimonate	
TN VG2	yellow	yellow green	65	−11	38	translucent	N	Mn-glass		
PN NC1	yellow	light amber	65	2	31	semi-opaque	N	Mn-glass	Pb-antimonate	
PN VP1	green	green	54	−28	19	opaque	N	Sb/Mn glass	Pb-antimonate	Cu
TN VP1	green	green	74	−27	29	opaque	N	Sb/Mn glass	Pb-antimonate	Cu
TN VP2	green	green	66	−21	41	opaque	N	Sb/Mn glass	Pb-antimonate	Cu
PN VS1	green	dark green	41	−29	1	opaque	N	Sb/Mn glass	Pb-antimonate	Cu
TN VS1	green	dark green	49	−22	5	translucent	N	Sb/Mn glass		Cu
TN VS2	green	dark green	50	−27	8	opaque	N	Sb/Mn glass	Pb-antimonate	Cu
PN VTR1	green	dark green	29	−25	8	translucent	N	Sb/Mn glass		Fe
PN VTR2	green	dark green	30	−25	4	translucent	N	Sb/Mn glass		Fe
TN VOL2	green	olive green	62	−10	35	translucent	N	n.a.		Cu
PN AV1	red	orange	63	33	66	opaque	N	n.a.	cuprite	
PN AV2	red	orange/red	58	34	59	opaque	N	n.a.	cuprite	
TN AV1	red	orange/red	66	38	58	opaque	N	n.a.	cuprite	
PN M1	red	brown	31	25	10	opaque	N	n.a.	metallic copper	
PN M2	red	brown	29	35	6	opaque	A?	n.a.	metallic copper	
TN M1	red	brown	22	26	21	opaque	N	n.a.	metallic copper	
TN M2	red	brown	33	32	15	opaque	N	n.a.	metallic copper	
TN M3	red	brown	39	41	29	opaque	N	n.a.	metallic copper	
PN M3	red	green red	72 33	−12 42	41 42	translucent with opaque bands	N	n.a. n.a.	metallic copper (red bands)	Cu (green glass)
TN VOL1	red	green red	61 40	−5 28	43 18	translucent with opaque bands	N	n.a. n.a.	metallic copper (red bands)	Cu (green glass)
TN NS1	red	dark amber	53	7	20	semi-opaque	N	Sb/Mn glass	metallic copper	

The mineralogical analysis of the opacifiers is carried out using X-ray powder diffraction (XRPD) and, in the case of orange/red-banded samples (PN AV2 and TN AV1), micro-XRD is performed on each color separately. There are two instruments employed: the first one is a PANalytical X'Pert PRO diffractometer (Bragg-Brentano geometry), equipped with a CuKα X-ray tube (1.5418 Å, 40 kV and 40 mA) and X'Celerator detector (Malvern Panalytical, Almelo, The Netherlands). The scans are collected in the angular range 3°–80° 2θ with a 0.03° virtual step size and a 100 s/step counting time. The second instrument, employed to have micro-diffraction patterns of the red and orange bands of samples PN AV2 and TN AV1, is a prototype consisting of an Agilent Supernova goniometer (Agilent Technologies, Santa Clara, CA, USA) equipped with an X-ray micro-source assembled with a Pilatus 200 K Dectris detector (DECTRIS Ltd., Baden-Daettwil, Switzerland). The micro-X-ray source, MoKα (0.7107 Å), operates at 50 kV and 0.8 mA, with a spot size of 0.11 mm. The sample-to-detector distance was 68 mm. The micro source ensures a brilliance at least ten times higher than conventional sealed X-ray tubes and a beam spot of ~0.120 mm. At the same time, the Pilatus 200 K detector ensures a very high sensitivity and negligible noise. The instrument is able to provide significant results on samples of extremely small size, down to 0.01 mm. In the present analyses, data were collected in micro-X-ray powder diffraction mode, simulating a Gandolfi camera measurement mode, due to the polycrystalline nature of the samples. Both XRPD and micro-XRD analytical data were processed by the X'Pert HighScore (PANalytical copyright); 2θ and d values were calculated with the second-derivative algorithm of Savitzky and Golay [32].

Reflectance spectra were acquired on some tesserae of blue and white macro-groups (TN AZ1, TN AZ2, PN GR1, TN GR1, TN GR2), to check the qualitative presence of cobalt by means of fiber-optic reflectance spectrometry (FORS). The instrument is an Ocean Optics Fiber Optic Reflectance spectrophotometer, consisting of a light source, an integrating sphere and a spectrometer, all connected by means of optical fibers (Ocean Optics, Largo, FL, USA). The light source is a deuterium-halogen lamp (DH-2000), generating radiation between 210 and 1500 nm, and the spectrometer is a wavelength dispersive system, mod. HR 2000+. The spectra were acquired between 188 and 1100 nm, with 10 replicas and an acquisition time of 60 s. For an objective color classification of tesserae from Pordenone and Trento, FORS was also used to determine the colorimetric coordinates of all but colorless macro-groups. The colorimetric coordinates are expressed in the CIELAB color space (L*, a*, b*), in accordance with the Italian Recommendation Normal 43/93.

Electron paramagnetic resonance (EPR) was employed to determine the oxidation state of iron in tesserae PN VTR1 and PN VTR2. EPR analyses were conducted with a Bruker ECS106 Electron Spin Resonance instrument with a TNH resonator and a frequency counter Hewlett Packard 5342 (Bruker, Billerica, MA, USA). All samples were acquired at room temperature under a microwave power of 20 mW, modulation amplitude of 8 G and microwave frequency of 9.55 GHz.

Micro-Raman spectroscopy was employed to clarify the crystalline phases used as opacifier in some white, turquoise, blue, yellow and green tesserae, when XRPD and SEM-EDS analyses were not completely resolutive. Raman spectra were obtained using a DXR Thermo Scientific Raman microscope, equipped with a diode-pumped solid state 532 nm laser, operating at a power of 8 mW (Thermo Fisher Scientific, Waltham, MA, USA). The analytical points were performed with a 50× LWD (Long Working Distance) objective, with a spatial resolution of about 1 μm and a spectral resolution in the range of 2.7–4.2 cm^{-1}. Data were collected in the 300–3500 cm^{-1} region, and the acquisition time adopted was 5 s for 32 scans accumulation.

The variety of techniques employed here required different procedures for sample preparation, which were conducted with the aim of preserving the tesserae as much as possible.

The tesserae were prepared in polished sections for the OM, SEM, EPMA and micro-Raman analyses and, in the case of SEM and EPMA, the sections were also coated with a thin carbon layer.

XRPD was performed on the whole tesserae, while for the micro-XRD of PN AV2 and TN AV1, micrometric fragments of each colored band were sampled and mounted on a capillary tube.

For the FORS analyses carried out on the whole tesserae, one surface of each sample was flattened and polished in order to guarantee maximum reflectance.

EPR was performed on millimetric fragments of the samples inserted in a quartz tube.

3. Results and Discussion

The results obtained with the Pordenone and Trento tesserae are reported in the following sub-sections, which separately discuss the glassy matrices and the various colors. The colors are grouped on the basis of the identified opacifiers, if any. Main results of the present study for each tessera are summarized in Table 1.

3.1. Glassy Matrices

The chemical analyses of the glassy matrices of all the tesserae from Pordenone and Trento, carried out by means of EPMA, are reported in Table 2.

All the samples, independent of provenance and color, are characterized by a soda content of ≈15–20 wt %, lime ≈ 5–8 wt %, low alumina (≈2–2.5 wt %), and potash and magnesia below 1.50 wt %, which are in line with the glassmaking tradition of natron-fluxed glass [33]. In only one brown tessera from Pordenone, labelled PN M2, potash and magnesia exceed the compositional limits of natron (Table 2) and are consistent with a plant-ash-based glass [33], which is seldom identified in deeply colored Roman glasses [34,35] or opaque red glasses dated to the Roman and Byzantine times [36].

In addition, the samples analyzed contain lead in variable concentrations, from negligible to up to ≈25 wt %, as PbO (Table 2). The highest lead contents are detected in the orange samples from Pordenone and a remarkable concentration (>5 wt % as PbO) is also identified in some tesserae of the red, yellow and green macro-groups. The present results show how the presence of lead is linked to the production of specific colors, such as red, green and yellow, and that very high lead (>20 wt % as PbO) is specifically used to produce orange tesserae. Further discussion on the role of lead in orange glass is presented in the sub-section on "red tesserae".

In order to determine the type of base glass used to make the tesserae from Pordenone and Trento, a so-called reduced composition of each glassy matrix is calculated, following the method reported in [11], because the intentional addition of lead, colorants and opacifiers (discussed in the next sub-sections) affects the original chemical compositions of tesserae, sometimes considerably. The reduced compositions are then compared against literature compositional groups for the period of interest; in particular, the main compositional groups dominating the Roman period (1st–3rd century AD) are Sb-colorless, Mn-colorless, Sb/Mn colorless, and unintentionally colored glass. They differ in antimony and manganese contents, being Sb-colorless characterized by high antimony content (Sb_2O_3 = 0.81 ± 0.16 wt %) and no manganese, Mn-colorless by very high manganese (MnO = 1.41 ± 0.27 wt %) and no antimony, Sb/Mn colorless glass by the presence of both manganese (MnO = 0.41 ± 0.16 wt %) and antimony (Sb_2O_3 = 0.43 ± 0.15 wt %), and unintentionally colored glass by generally low manganese (MnO < 1 wt %) and negligible antimony [37–39]. In addition to different ratios of manganese and antimony, which are not considered in the reduced compositions, the other key characteristics of these groups are the different contents of SiO_2, Na_2O, CaO and Al_2O_3 [37,39]: Sb-colorless glass is characterized by high silica and soda (SiO_2: 69 ÷ 73 wt %; Na_2O: 18.5 ÷ 20.5 wt %) and low lime and alumina (CaO: 4 ÷ 5.5 wt % and Al_2O_3: 1.6 ÷ 2.2 wt %), Mn-colorless and unintentionally colored glass by low silica and soda (SiO_2: 67 ÷ 71 wt %; Na_2O: 14.5 ÷ 17 wt %) and high lime and alumina (CaO: 7 ÷ 9. wt % and Al_2O_3: 2.5 ÷ 3 wt %), and Sb/Mn colorless glass by intermediate contents of the above elements (SiO_2: 68.5 ÷ 71 wt %; Na_2O: 16.5 ÷ 18.5 wt %; CaO: 5.5 ÷ 7 wt %; Al_2O_3: 2 ÷ 2.5 wt %). Therefore, the Roman compositional groups are here referred as Sb-glass, Sb/Mn glass and Mn-glass (the last including both Mn-colorless glass and unintentionally colored glass).

Table 2. The mean chemical compositions of the glass tesserae (EPMA data, expressed as weight percentage of the corresponding oxide, except for chlorine; standard deviation in italics). Color macro-group, color, diaphaneity reported for each sample.

Sample	Color Macro-Group	Color	Diaphaneity	SiO_2	Na_2O	CaO	Al_2O_3	MnO	Fe_2O_3	MgO	K_2O	TiO_2	P_2O_5	SO_3	Cl	CoO	CuO	ZnO	SnO_2	Sb_2O_3	PbO	TOT
PN AU1	colorless	gold	transparent	69.35	16.22	7.97	2.26	1.90	0.37	0.64	0.55	0.05	0.09	0.12	1.24	<0.03	<0.03	<0.04	<0.04	<0.04	<0.08	100.76
				0.28	*0.30*	*0.09*	*0.11*	*0.28*	*0.05*	*0.01*	*0.06*	*0.01*	*0.03*	*0.04*	*0.05*							
PN AU1 (cart)	colorless	gold	transparent	69.49	16.20	8.00	2.24	1.73	0.41	0.66	0.50	0.06	0.09	0.11	1.30	<0.03	<0.03	<0.04	<0.04	<0.04	<0.08	100.79
				0.28	*0.17*	*0.01*	*0.13*	*0.11*	*0.02*	*0.02*	*0.03*	*0.00*	*0.02*	*0.01*	*0.00*							
PN AU2	colorless	gold	transparent	68.91	16.26	7.99	2.30	1.80	0.36	0.67	0.55	0.08	0.09	0.13	1.26	<0.03	<0.03	<0.04	<0.04	<0.04	<0.08	100.40
				0.19	*0.24*	*0.09*	*0.09*	*0.12*	*0.02*	*0.01*	*0.04*	*0.02*	*0.01*	*0.01*	*0.02*							
PN AU2 (cart)	colorless	gold	transparent	69.45	16.29	7.99	2.31	1.87	0.37	0.65	0.53	0.06	0.09	0.12	1.21	<0.03	<0.03	<0.04	<0.04	<0.04	<0.08	100.96
				0.29	*0.18*	*0.09*	*0.06*	*0.03*	*0.06*	*0.05*	*0.03*	*0.02*	*0.02*	*0.01*	*0.02*							
TN AU1	colorless	gold	transparent	72.10	15.09	8.01	2.43	0.38	0.31	0.53	0.42	0.07	0.10	0.16	1.11	<0.03	<0.03	<0.04	<0.04	<0.04	<0.08	100.72
				0.41	*0.29*	*0.11*	*0.02*	*0.14*	*0.03*	*0.00*	*0.05*	*0.01*	*0.04*	*0.02*	*0.04*							
TN AU1 (cart)	colorless	gold	transparent	71.99	15.14	7.84	2.39	0.35	0.33	0.53	0.42	0.07	0.08	0.15	1.11	<0.03	<0.03	<0.04	<0.04	<0.04	<0.08	100.38
				0.27	*0.22*	*0.04*	*0.15*	*0.04*	*0.02*	*0.02*	*0.02*	*0.02*	*0.02*	*0.02*	*0.03*							
PN AG1	colorless	colorless	transparent	69.26	16.29	8.01	2.25	1.77	0.38	0.65	0.54	0.06	0.09	0.13	1.29	<0.03	<0.03	<0.04	<0.04	<0.04	<0.08	100.72
				0.38	*0.16*	*0.08*	*0.09*	*0.07*	*0.02*	*0.02*	*0.05*	*0.01*	*0.02*	*0.03*	*0.04*							
TN TR INC 1	colorless	colorless	transparent	68.04	18.87	7.20	2.11	0.01	0.56	0.68	0.57	0.09	0.03	0.31	1.36	<0.03	<0.03	<0.04	<0.04	0.66	<0.08	100.50
				0.37	*0.16*	*0.08*	*0.13*	*0.01*	*0.04*	*0.02*	*0.07*	*0.01*	*0.03*	*0.02*	*0.03*					*0.04*		
PN TU1	turquoise	turquoise	opaque	65.27	15.72	6.75	2.39	0.63	0.69	0.93	0.84	0.09	0.30	0.38	0.81	<0.03	2.89	<0.04	0.29	2.52	0.40	100.90
				0.63	*0.24*	*0.05*	*0.10*	*0.04*	*0.04*	*0.05*	*0.07*	*0.01*	*0.02*	*0.02*	*0.03*		*0.80*		*0.08*	*0.42*	*0.05*	
PN TU2 (tr)	turquoise	turquoise	translucent	62.86	17.83	5.54	2.52	0.22	0.88	0.87	0.69	0.13	0.31	0.37	1.15	<0.03	4.49	0.11	0.14	1.45	1.21	100.77
				1.87	*0.27*	*0.16*	*0.26*	*0.05*	*0.15*	*0.08*	*0.09*	*0.02*	*0.04*	*0.04*	*0.05*		*0.55*	*0.05*	*0.10*	*0.37*	*0.56*	
PN TU2 (op)	turquoise	turquoise	opaque	64.86	17.71	5.32	2.21	0.14	0.74	0.67	0.56	0.11	0.11	0.41	1.10	<0.03	3.08	0.06	0.09	2.56	0.89	100.63
				1.35	*0.35*	*0.05*	*0.02*	*0.05*	*0.01*	*0.01*	*0.05*	*0.03*	*0.02*	*0.04*	*0.06*		*0.64*	*0.01*	*0.05*	*0.65*	*0.05*	
PN TU3	turquoise	turquoise	opaque	68.09	17.53	4.52	2.02	<0.05	0.52	0.39	0.50	0.07	0.01	0.21	1.38	<0.03	2.83	0.10	0.21	1.89	0.31	100.60
				0.24	*0.14*	*0.03*	*0.10*		*0.04*	*0.02*	*0.03*	*0.03*	*0.02*	*0.02*	*0.01*		*0.07*	*0.03*	*0.01*	*0.02*	*0.05*	
TN TU1	turquoise	turquoise	opaque	65.13	16.11	7.22	2.50	0.73	0.67	0.70	0.72	0.09	0.20	0.39	0.89	<0.03	2.32	<0.04	0.22	1.64	0.40	99.92
				0.45	*0.21*	*0.10*	*0.10*	*0.03*	*0.02*	*0.03*	*0.07*	*0.01*	*0.02*	*0.02*	*0.02*		*0.05*		*0.01*	*0.28*	*0.04*	
TN TU2	turquoise	turquoise	opaque	64.49	15.93	5.69	2.43	0.61	0.70	0.74	0.63	0.13	0.06	0.34	1.09	<0.03	4.49	<0.04	0.24	3.06	0.72	101.36
				0.94	*0.24*	*0.17*	*0.19*	*0.03*	*0.03*	*0.03*	*0.10*	*0.03*	*0.04*	*0.02*	*0.04*		*0.09*		*0.03*	*1.76*	*0.05*	
TN TU3	turquoise	turquoise	opaque	64.95	16.03	7.25	2.44	0.74	0.66	0.71	0.70	0.09	0.18	0.39	0.89	<0.03	2.34	<0.04	0.21	1.78	0.41	99.78
				0.58	*0.28*	*0.08*	*0.15*	*0.05*	*0.04*	*0.04*	*0.02*	*0.02*	*0.02*	*0.02*	*0.02*		*0.06*		*0.03*	*0.50*	*0.05*	
TN BS1	turquoise	dark blue	translucent	64.50	17.55	5.95	2.36	0.53	0.81	0.70	0.68	0.14	0.22	0.28	1.34	<0.03	5.07	<0.04	0.13	0.56	0.26	101.07
				0.55	*0.21*	*0.10*	*0.04*	*0.05*	*0.03*	*0.02*	*0.05*	*0.00*	*0.02*	*0.01*	*0.04*		*0.89*		*0.07*	*0.06*	*0.06*	
PN BS1	turquoise	dark blue	translucent	66.89	19.32	5.85	2.16	0.57	0.63	0.65	0.61	0.11	0.11	0.31	1.39	<0.03	1.81	<0.04	0.14	0.62	0.09	101.28
				0.59	*0.33*	*0.18*	*0.10*	*0.05*	*0.05*	*0.02*	*0.04*	*0.01*	*0.02*	*0.05*	*0.06*		*0.66*		*0.03*	*0.02*	*0.04*	
PN CE1	turquoise	pale blue	opaque	65.36	15.58	6.37	2.75	0.43	0.98	0.74	0.68	0.11	0.18	0.41	0.73	<0.03	2.21	<0.04	0.10	3.74	0.13	100.50
				0.38	*0.21*	*0.15*	*0.12*	*0.04*	*0.05*	*0.04*	*0.03*	*0.02*	*0.03*	*0.08*	*0.04*		*0.34*		*0.06*	*0.35*	*0.01*	
TN CE1	turquoise	pale blue	opaque	63.88	16.76	6.62	2.66	0.23	0.98	0.79	0.67	0.11	0.18	0.47	0.87	<0.03	2.70	<0.04	0.14	3.02	0.09	100.17
				0.40	*0.35*	*0.11*	*0.11*	*0.03*	*0.06*	*0.02*	*0.04*	*0.01*	*0.02*	*0.02*	*0.03*		*0.04*		*0.04*	*0.21*	*0.05*	
PN AQ1	turquoise	aquamarine	semi-opaque	66.04	17.70	6.51	2.42	0.40	0.74	0.74	0.68	0.12	0.17	0.29	1.29	<0.03	2.30	<0.04	0.11	0.79	0.20	100.50
				0.62	*0.23*	*0.08*	*0.11*	*0.03*	*0.06*	*0.02*	*0.05*	*0.03*	*0.02*	*0.03*	*0.03*		*0.05*		*0.03*	*0.12*	*0.07*	
TN AQ1	turquoise	aquamarine	opaque	66.37	16.62	7.00	2.48	0.89	0.52	0.64	0.69	0.09	0.06	0.28	1.23	<0.03	2.42	<0.04	0.19	0.83	0.33	100.67
				0.49	*0.30*	*0.09*	*0.17*	*0.03*	*0.03*	*0.04*	*0.10*	*0.02*	*0.04*	*0.02*	*0.06*		*0.08*		*0.03*	*0.16*	*0.08*	
TN AQ2	turquoise	aquamarine	opaque	66.28	16.87	7.06	2.41	0.85	0.58	0.69	0.68	0.10	0.17	0.30	1.07	<0.03	2.17	<0.04	0.16	0.69	0.28	100.36
				0.71	*0.16*	*0.16*	*0.09*	*0.05*	*0.06*	*0.03*	*0.05*	*0.02*	*0.02*	*0.01*	*0.05*		*0.26*		*0.05*	*0.13*	*0.07*	
PN VCH1	turquoise	pale green	opaque	68.21	18.29	6.67	2.26	0.58	0.44	0.68	0.54	0.08	0.10	0.26	1.24	<0.03	0.68	<0.03	<0.04	0.88	<0.08	100.91
				0.34	*0.25*	*0.05*	*0.07*	*0.04*	*0.03*	*0.03*	*0.04*	*0.01*	*0.02*	*0.02*	*0.03*		*0.03*			*0.06*		

Table 2. *Cont.*

Sample	Color Macro-Group	Color	Diaphaneity	SiO_2	Na_2O	CaO	Al_2O_3	MnO	Fe_2O_3	MgO	K_2O	TiO_2	P_2O_5	SO_3	Cl	CoO	CuO	ZnO	SnO_2	Sb_2O_3	PbO	TOT
TN VCH1	turquoise	pale green	opaque	64.06	17.23	6.53	2.51	0.20	0.91	0.77	0.62	0.12	0.14	0.40	1.01	<0.03	2.84	<0.04	0.16	3.22	0.12	100.85
				1.02	*0.34*	*0.15*	*0.08*	*0.01*	*0.01*	*0.01*	*0.04*	*0.01*	*0.04*	*0.01*	*0.04*		*0.08*		*0.02*	*0.62*	*0.02*	
PN BO1	blue	blue	opaque	66.11	15.06	6.70	2.49	0.63	1.12	0.80	0.74	0.09	0.24	0.42	0.68	0.17	0.26	<0.04	<0.04	4.40	0.11	100.03
				0.35	*0.40*	*0.06*	*0.15*	*0.04*	*0.08*	*0.02*	*0.03*	*0.02*	*0.02*	*0.02*	*0.01*	*0.03*	*0.02*			*0.06*	*0.03*	
TN BO1	blue	blue	opaque	68.95	16.40	7.06	2.32	0.78	0.84	0.63	0.59	0.07	0.19	0.24	1.15	0.10	0.17	<0.04	<0.04	0.76	<0.08	100.25
				1.39	*0.36*	*0.21*	*0.10*	*0.15*	*0.39*	*0.06*	*0.04*	*0.01*	*0.03*	*0.05*	*0.14*	*0.05*	*0.02*			*0.87*		
TN B1	blue	blue	translucent	69.42	18.18	6.61	1.93	1.54	0.48	0.53	0.43	0.05	0.17	0.17	1.63	0.06	0.06	<0.04	<0.04	<0.04	<0.08	101.24
				0.35	*0.17*	*0.04*	*0.08*	*0.08*	*0.06*	*0.03*	*0.03*	*0.01*	*0.02*	*0.04*	*0.05*	*0.01*	*0.02*					
PN AZ1	blue	azure	opaque	61.01	15.96	7.68	2.33	1.16	1.89	0.64	0.58	0.03	0.21	0.57	0.69	0.19	0.57	<0.04	<0.04	6.39	<0.08	99.90
				0.59	*0.27*	*0.15*	*0.11*	*0.04*	*0.07*	*0.03*	*0.03*	*0.02*	*0.02*	*0.05*	*0.02*	*0.02*	*0.02*			*0.57*		
PN AZ2	blue	azure	translucent with opaque bands	68.47	15.13	8.69	2.47	0.87	0.68	0.63	0.53	0.06	0.22	0.32	0.95	0.03	0.04	<0.04	<0.04	1.37	<0.08	100.48
				0.22	*0.23*	*0.15*	*0.12*	*0.15*	*0.08*	*0.04*	*0.04*	*0.02*	*0.03*	*0.05*	*0.04*	*0.01*	*0.02*			*0.30*		
TN AZ1	blue	azure	opaque	67.52	16.12	7.24	2.49	0.81	0.63	0.67	0.68	0.07	0.17	0.40	0.85	<0.03	0.15	<0.04	<0.04	2.49	0.19	100.48
				0.49	*0.20*	*0.07*	*0.03*	*0.05*	*0.03*	*0.02*	*0.09*	*0.01*	*0.02*	*0.03*	*0.03*		*0.01*			*0.18*	*0.04*	
TN AZ2	blue	azure	opaque	67.47	16.24	6.76	2.37	0.57	0.82	0.69	0.60	0.10	0.19	0.42	0.94	0.03	0.12	<0.04	<0.04	2.88	0.29	100.50
				0.34	*0.28*	*0.10*	*0.08*	*0.02*	*0.04*	*0.03*	*0.03*	*0.02*	*0.02*	*0.10*	*0.06*		*0.02*			*0.13*	*0.07*	
PN BIOP1	white	white	opaque	67.82	14.89	5.85	1.99	0.66	0.39	0.46	0.54	0.04	0.18	0.36	0.63	<0.03	<0.3	<0.04	<0.04	4.67	1.29	99.78
				0.54	*0.17*	*0.05*	*0.09*	*0.03*	*0.02*	*0.02*	*0.09*	*0.01*	*0.02*	*0.03*	*0.02*					*0.18*	*0.13*	
TN BIOP1	white	white	opaque	67.39	15.64	7.28	2.63	0.80	0.64	0.66	0.74	0.08	0.08	0.39	0.83	<0.03	0.07	<0.04	<0.04	2.88	0.23	100.32
				1.11	*0.45*	*0.11*	*0.10*	*0.03*	*0.08*	*0.03*	*0.07*	*0.02*	*0.03*	*0.18*	*0.15*		*0.04*			*1.24*	*0.18*	
PN GR1	white	grey	opaque	67.48	17.91	6.73	2.46	0.59	0.74	0.73	0.69	0.11	0.20	0.29	1.14	<0.03	0.04	<0.04	<0.04	1.29	<0.08	100.39
				0.37	*0.13*	*0.04*	*0.13*	*0.02*	*0.02*	*0.02*	*0.09*	*0.02*	*0.02*	*0.03*	*0.01*		*0.01*			*0.07*		
TN GR1	white	grey	opaque	67.80	17.14	6.57	2.32	0.31	0.70	0.76	0.71	0.09	0.06	0.34	0.95	<0.03	0.03	<0.04	<0.04	2.60	<0.08	100.38
				0.35	*0.17*	*0.08*	*0.08*	*0.04*	*0.04*	*0.05*	*0.05*	*0.02*	*0.02*	*0.02*	*0.03*		*0.01*			*0.28*		
TN GR2	white	grey	opaque	69.12	16.35	6.86	2.39	0.55	0.69	0.73	0.58	0.10	0.11	0.25	1.05	<0.03	0.06	<0.04	<0.04	1.49	0.19	100.50
				0.14	*0.31*	*0.06*	*0.11*	*0.03*	*0.05*	*0.03*	*0.07*	*0.02*	*0.03*	*0.02*	*0.01*		*0.02*			*0.11*	*0.02*	
PN GSO1	yellow	yellow	opaque	66.22	17.28	4.99	2.10	0.67	0.88	0.66	0.62	0.14	0.08	0.28	0.99	<0.03	<0.03	<0.03	<0.04	0.85	3.76	99.51
				0.34	*0.22*	*0.07*	*0.13*	*0.03*	*0.09*	*0.03*	*0.05*	*0.02*	*0.03*	*0.02*	*0.04*					*0.04*	*0.48*	
PN GSO2 (tr)	yellow	yellow	translucent	65.67	15.88	7.04	2.16	0.54	0.58	0.48	0.54	0.06	0.11	0.22	1.00	<0.03	<0.03	<0.04	0.10	0.52	5.11	99.98
				0.55	*0.29*	*0.18*	*0.08*	*0.07*	*0.19*	*0.02*	*0.04*	*0.02*	*0.01*	*0.02*	*0.06*				*0.06*	*0.30*	*0.14*	
PN GSO2 (op)	yellow	yellow	opaque	61.23	13.76	6.76	2.23	0.44	0.95	0.49	0.49	0.07	0.06	0.17	0.90	<0.03	<0.03	<0.04	0.09	0.25	11.52	99.39
				2.97	*0.53*	*0.17*	*0.07*	*0.06*	*0.82*	*0.03*	*0.11*	*0.01*	*0.02*	*0.05*	*0.10*				*0.02*	*0.32*	*1.37*	
TN GSO1	yellow	yellow	opaque	68.88	17.55	6.67	2.13	1.09	0.26	0.57	0.53	0.08	0.04	0.29	1.20	<0.03	<0.03	<0.04	<0.04	0.45	0.51	100.26
				0.44	*0.28*	*0.10*	*0.11*	*0.08*	*0.22*	*0.02*	*0.04*	*0.02*	*0.03*	*0.03*	*0.04*					*0.04*	*0.10*	
TN GSO2	yellow	yellow	opaque	66.86	16.56	6.45	2.28	0.78	0.45	0.53	0.57	0.11	0.05	0.26	1.13	<0.03	<0.03	<0.04	0.09	0.49	3.63	100.23
				0.46	*0.25*	*0.08*	*0.07*	*0.05*	*0.17*	*0.02*	*0.04*	*0.10*	*0.04*	*0.02*	*0.03*				*0.05*	*0.15*	*0.21*	
PN VG1	yellow	yellow-green	opaque	67.12	16.04	6.34	2.30	0.72	0.93	0.76	0.78	0.13	0.21	0.19	0.95	<0.03	0.04	<0.04	0.11	0.34	3.59	100.54
				0.37	*0.16*	*0.11*	*0.11*	*0.03*	*0.06*	*0.03*	*0.05*	*0.01*	*0.02*	*0.01*	*0.03*		*0.02*		*0.08*	*0.16*	*0.38*	
TN VG1	yellow	yellow-green	semi-opaque	66.25	16.38	6.94	2.26	0.43	1.36	0.84	0.72	0.09	0.15	0.29	1.22	<0.03	0.59	<0.04	0.09	0.64	2.27	100.52
				0.16	*0.19*	*0.10*	*0.10*	*0.05*	*0.03*	*0.03*	*0.06*	*0.01*	*0.02*	*0.03*	*0.02*		*0.04*		*0.02*	*0.06*	*0.10*	
TN VG2	yellow	yellow- green	translucent	67.10	15.89	7.52	2.82	0.97	1.59	0.77	0.86	0.10	0.12	0.28	1.05	<0.03	0.89	<0.04	0.04	0.44	0.50	100.94
				0.29	*0.29*	*0.13*	*0.15*	*0.04*	*0.08*	*0.03*	*0.04*	*0.01*	*0.03*	*0.02*	*0.04*		*0.09*		*0.02*	*0.04*	*0.07*	
PN NC1	yellow	light amber	semi-opaque	68.67	16.76	6.88	2.41	0.35	0.51	0.59	0.56	0.09	0.09	0.19	1.21	<0.03	<0.03	<0.04	<0.04	0.26	1.82	100.38
				0.41	*0.20*	*0.14*	*0.09*	*0.03*	*0.05*	*0.02*	*0.05*	*0.02*	*0.03*	*0.04*	*0.05*					*0.03*	*0.26*	
PN VP1	green	green	opaque	66.11	17.30	6.46	2.48	0.50	0.60	0.67	0.69	0.11	0.11	0.24	1.21	<0.03	1.06	<0.04	0.06	0.38	2.50	100.48
				0.54	*0.26*	*0.07*	*0.09*	*0.02*	*0.03*	*0.03*	*0.06*	*0.02*	*0.02*	*0.03*	*0.04*		*0.04*		*0.03*	*0.06*	*0.41*	

Table 2. *Cont.*

Sample	Color Macro-Group	Color	Diaphaneity	SiO_2	Na_2O	CaO	Al_2O_3	MnO	Fe_2O_3	MgO	K_2O	TiO_2	P_2O_5	SO_3	Cl	CoO	CuO	ZnO	SnO_2	Sb_2O_3	PbO	TOT
TN VP1	green	green	opaque	64.83	16.47	6.63	2.38	0.62	0.74	0.67	0.65	0.10	0.12	0.23	1.18	<0.03	1.13	<0.04	0.13	0.56	3.58	100.00
				0.46	*0.22*	*0.10*	*0.07*	*0.04*	*0.05*	*0.02*	*0.04*	*0.01*	*0.01*	*0.03*	*0.06*		*0.05*		*0.03*	*0.04*	*0.20*	
TN VP2	green	green	opaque	64.91	16.35	6.54	2.30	0.61	0.69	0.62	0.65	0.11	0.12	0.24	1.18	<0.03	0.97	<0.4	0.16	0.66	3.99	100.09
				0.64	*0.26*	*0.06*	*0.13*	*0.06*	*0.04*	*0.02*	*0.06*	*0.02*	*0.02*	*0.03*	*0.05*		*0.08*		*0.10*	*0.19*	*0.49*	
PN VS1	green	dark green	opaque	66.04	17.54	6.36	2.43	0.44	0.64	0.72	0.73	0.12	0.13	0.24	1.23	<0.03	2.52	<0.04	0.10	0.41	1.26	100.92
				0.24	*0.30*	*0.06*	*0.09*	*0.03*	*0.04*	*0.02*	*0.05*	*0.01*	*0.02*	*0.04*	*0.04*		*0.13*		*0.03*	*0.05*	*0.20*	
TN VS1	green	dark green	translucent	66.32	17.51	7.10	2.44	0.34	0.98	0.71	0.71	0.11	0.14	0.28	1.24	<0.03	1.84	<0.04	0.10	0.72	0.49	101.04
				0.53	*0.34*	*0.03*	*0.15*	*0.03*	*0.03*	*0.01*	*0.05*	*0.01*	*0.03*	*0.01*	*0.03*		*0.07*		*0.01*	*0.02*	*0.06*	
TN VS2	green	dark green	opaque	66.42	16.67	6.97	2.42	0.76	0.76	0.66	0.62	0.10	0.13	0.23	1.21	<0.03	1.70	<0.04	0.11	0.50	1.07	100.35
				0.22	*0.29*	*0.17*	*0.08*	*0.05*	*0.03*	*0.03*	*0.06*	*0.02*	*0.03*	*0.02*	*0.04*		*0.10*		*0.03*	*0.03*	*0.13*	
PN VTR1	green	dark green	translucent	62.59	16.20	6.19	2.07	0.77	1.92	0.54	0.55	0.07	0.10	0.20	1.13	<0.03	<0.03	<0.04	0.13	0.38	7.25	100.09
				1.13	*0.27*	*0.26*	*0.18*	*0.11*	*0.39*	*0.03*	*0.05*	*0.02*	*0.02*	*0.02*	*0.03*				*0.05*	*0.08*	*1.25*	
PN VTR2	green	dark green	translucent	63.50	16.00	6.34	2.19	0.92	2.79	0.57	0.56	0.09	0.09	0.20	1.13	<0.03	<0.03	<0.04	0.11	0.31	5.37	100.16
				1.05	*0.28*	*0.06*	*0.08*	*0.04*	*0.76*	*0.02*	*0.06*	*0.02*	*0.02*	*0.02*	*0.04*				*0.02*	*0.05*	*0.14*	
TN VOL2	green	olive green	translucent	59.35	12.89	6.89	2.94	1.28	2.46	0.69	0.83	0.11	0.12	0.31	0.80	<0.03	2.07	<0.04	0.40	0.77	8.45	100.34
				0.47	*0.37*	*0.07*	*0.14*	*0.13*	*0.10*	*0.04*	*0.07*	*0.02*	*0.03*	*0.03*	*0.04*		*0.07*		*0.03*	*0.05*	*0.21*	
PN AV1	red	orange	opaque	41.67	10.03	6.29	2.65	0.26	1.99	1.35	0.85	0.24	0.43	0.33	0.74	<0.03	8.34	<0.04	1.36	0.56	23.88	100.98
				0.37	*0.25*	*0.06*	*0.18*	*0.02*	*0.08*	*0.03*	*0.05*	*0.01*	*0.05*	*0.03*	*0.03*		*1.28*		*0.06*	*0.04*	*0.18*	
PN AV2 (or)	red	orange	opaque	43.25	9.71	6.19	2.52	0.28	1.20	0.71	0.64	0.14	0.16	0.38	0.56	<0.03	8.94	0.15	1.00	1.40	23.41	100.67
				0.31	*0.21*	*0.07*	*0.10*	*0.04*	*0.03*	*0.03*	*0.06*	*0.02*	*0.03*	*0.01*	*0.02*		*0.19*	*0.02*	*0.02*	*0.04*	*0.22*	
PN AV2 (red)	red	red	opaque	42.57	9.86	6.00	2.43	0.27	1.16	0.69	0.64	0.12	0.14	0.36	0.56	<0.03	7.71	0.13	0.97	1.38	25.48	100.49
				0.87	*0.26*	*0.25*	*0.12*	*0.03*	*0.07*	*0.05*	*0.03*	*0.04*	*0.03*	*0.06*	*0.03*		*1.15*	*0.01*	*0.02*	*0.09*	*0.93*	
TN AV1 (or)	red	orange	opaque	50.62	11.67	7.03	2.05	0.27	1.28	1.92	1.47	0.18	0.65	0.54	0.80	<0.03	14.14	0.07	1.01	0.96	6.07	100.74
				0.73	*0.32*	*0.06*	*0.09*	*0.02*	*0.05*	*0.04*	*0.10*	*0.02*	*0.03*	*0.04*	*0.01*		*0.48*	*0.03*	*0.03*	*0.03*	*0.20*	
TN AV1 (red)	red	red	opaque	52.13	12.94	7.26	2.11	0.28	1.36	1.94	1.45	0.17	0.62	0.49	0.85	<0.03	10.94	0.06	1.01	0.91	6.33	100.86
				1.02	*0.41*	*0.08*	*0.11*	*0.03*	*0.06*	*0.05*	*0.09*	*0.02*	*0.05*	*0.05*	*0.03*		*0.67*	*0.03*	*0.09*	*0.09*	*0.22*	
PN M1	red	brown	opaque	61.57	15.37	7.13	2.84	0.44	1.24	0.82	0.77	0.15	0.15	0.11	0.88	<0.03	1.27	0.19	0.34	0.40	6.27	99.95
				0.79	*0.26*	*0.10*	*0.10*	*0.03*	*0.08*	*0.03*	*0.04*	*0.02*	*0.04*	*0.03*	*0.10*		*0.26*	*0.05*	*0.06*	*0.02*	*0.57*	
PN M2	red	brown	opaque	61.59	15.83	7.85	2.06	0.65	1.61	3.05	2.14	0.19	1.21	0.52	1.20	<0.03	1.62	0.04	0.19	0.85	0.83	101.44
				0.63	*0.30*	*0.12*	*0.08*	*0.05*	*0.06*	*0.10*	*0.08*	*0.02*	*0.08*	*1.07*	*0.05*		*1.47*	*0.02*	*0.09*	*0.18*	*0.09*	
TN M1	red	brown	opaque	62.84	14.51	7.01	2.73	0.84	4.10	0.81	0.85	0.10	0.18	0.28	0.98	<0.03	0.74	<0.04	0.24	0.64	3.61	100.47
				0.54	*0.44*	*0.26*	*0.21*	*0.06*	*0.13*	*0.02*	*0.06*	*0.02*	*0.03*	*0.03*	*0.02*		*0.13*		*0.04*	*0.02*	*0.25*	
TN M2 (dark)	red	brown	opaque	62.82	14.36	6.97	2.84	0.86	3.89	0.81	0.80	0.11	0.16	0.27	0.94	<0.03	0.47	<0.04	0.21	0.75	4.65	100.91
				0.79	*0.42*	*0.17*	*0.12*	*0.04*	*0.52*	*0.03*	*0.03*	*0.03*	*0.02*	*0.04*	*0.07*		*0.29*		*0.07*	*0.14*	*1.09*	
TN M2 (pale)	red	brown	opaque	62.76	14.01	7.10	2.75	0.87	2.71	0.81	0.87	0.10	0.15	0.29	0.93	<0.03	0.58	<0.04	0.17	0.85	5.40	100.35
				1.25	*0.39*	*0.19*	*0.15*	*0.05*	*0.42*	*0.02*	*0.08*	*0.02*	*0.03*	*0.03*	*0.03*		*0.10*		*0.04*	*0.16*	*0.97*	
TN M3	red	brown	opaque	60.61	15.31	6.27	2.60	0.34	2.62	0.75	0.79	0.11	0.11	0.27	0.96	<0.03	0.61	<0.04	0.31	0.68	8.09	100.42
				0.30	*0.14*	*0.49*	*0.11*	*0.04*	*0.10*	*0.02*	*0.04*	*0.02*	*0.03*	*0.02*	*0.05*		*0.37*		*0.05*	*0.03*	*0.32*	
PN M3	red	green/red	translucent with opaque bands	51.78	12.76	7.58	2.79	0.34	1.42	0.92	0.78	0.16	0.16	0.18	0.98	<0.03	2.48	0.06	0.39	0.78	15.66	99.20
				0.30	*0.34*	*0.26*	*0.13*	*0.02*	*0.06*	*0.02*	*0.09*	*0.03*	*0.04*	*0.03*	*0.15*		*0.19*	*0.02*	*0.03*	*0.04*	*0.50*	
TN VOL 1	red	green/red	translucent with opaque bands	66.44	16.11	6.81	2.78	0.58	1.91	0.90	0.81	0.16	0.17	0.27	1.11	<0.03	1.37	<0.04	0.15	0.57	0.87	101.00
				0.28	*0.17*	*0.15*	*0.35*	*0.03*	*0.21*	*0.05*	*0.09*	*0.01*	*0.04*	*0.04*	*0.08*		*0.47*		*0.03*	*0.05*	*0.16*	
TN NS1	red	dark amber	semi-opaque	66.04	16.77	6.35	2.31	0.64	1.59	0.73	0.74	0.10	0.10	0.28	1.08	<0.03	0.66	<0.04	0.06	0.66	2.38	100.50
				0.48	*0.23*	*0.25*	*0.09*	*0.05*	*0.03*	*0.02*	*0.06*	*0.02*	*0.04*	*0.03*	*0.04*		*0.03*		*0.01*	*0.03*	*0.10*	

When examined in their reduced composition and neglecting the probable plant-ash based glass (PN M2), all the samples from Pordenone and Trento, except the red macro-group, are consistent with the considered Roman groups. The majority of the samples fit Sb/Mn glass and Mn-glass, except for samples TN TRINC1 (colorless) and PN TU3 (turquoise), which are similar to Sb-glass (Figure 2). As regards the remaining colorless tesserae, it is interesting to note that they are comparable with Mn-glass (Figure 2), and if the Mn contents are also taken into account (Table 2), all the three colorless tesserae from Pordenone are similar to Roman Mn-colorless glass, while TN AU1 to the unintentionally colored composition. Turquoise, white, and blue tesserae were made starting from both Sb/Mn and Mn-glass, while the majority of green and yellow tesserae were produced using Sb/Mn glass as a base (Table 1—Figure 2).

Taking into account that Sb/Mn and Mn-glass groups were used for lower value items and were widely available around the Mediterranean and continental Europe, the present results confirm the preference for the most readily available and least costly glass types as base glass of tesserae, as already verified in Roman assemblage from UK [12]. All the red macro-group (in particular, the orange tesserae), except for tessera TN NS1, does not fit the Roman compositional groups, mainly due to higher alumina and lime and lower silica contents (Figure 2), as well as magnesia, potash, and phosphorus oxide. Unfortunately, it is not possible to define how this difference is due to a different base glass, as such elements may have been influenced by the coloring technique that will be discussed in the sub-section on "red tesserae". It should be only stressed here that similar characteristics were highlighted in other Roman and Byzantine orange samples, and they could be related to the use of specific primary batches for the production of this color [36].

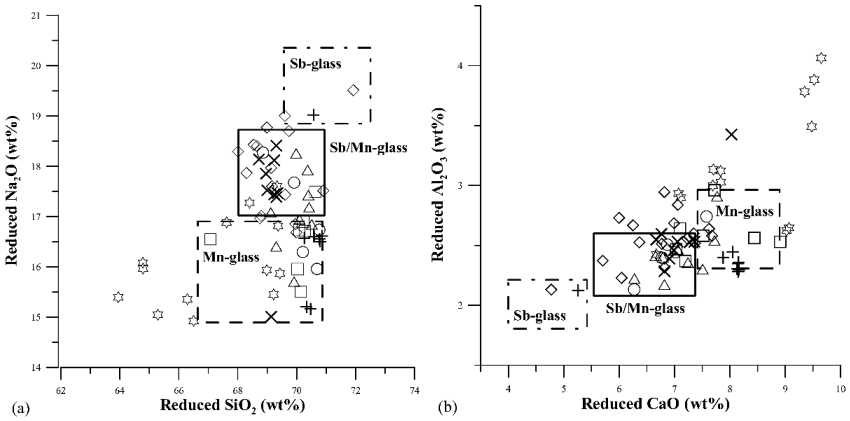

Figure 2. Reduced Na_2O *versus* SiO_2 (**a**) and reduced Al_2O_3 *versus* CaO (**b**) contents of Pordenone and Trento tesserae, subdivided by color macro-group: colorless (+), turquoise (◇), blue (□), white (○), yellow (△), green (×), red (✡). Compositional ranges of literature groups (Sb-glass; Sb/Mn glass; Mn-glass) calculated from raw data published in Silvestri [40], Silvestri et al. [41], Gallo et al. [42] and Maltoni et al. [43].

3.2. Colorless Tesserae

Colorless glass in mosaics is used only in the production of "gold" tesserae, in which a metal foil is enclosed between the supporting tessera and the covering layer or *cartellina*. In the present study, 5 colorless tesserae (3 from Pordenone and 2 from Trento) are selected (Table 1): three samples, PN AU1, PN AU2 and TN AU1, are complete tesserae, i.e., composed of supporting tesserae, gold foil and *cartellina*. PN AG1 does not present any metal foil between the tessera and the *cartellina*, even though it is perfectly preserved. Tessera TN TR INC1 is a former gold tessera that lost both its gold foil and *cartellina*. All the tesserae are entirely colorless, except for the presence of a purple translucent stripe in PN AU2 (Figure 1a), probably due to a local change in the oxidation state of Mn, which can be used as a decolorizer or as an ionic colorant [26].

When present, each tessera and its *cartellina* are made with the same glass. In detail, the three samples from Pordenone (PN AU1, PN AU2 and PN AG1) are compositionally very close (i.e., variability of EPMA data is within the precision of the method for all the considered elements—see Table 2), and probably derive from a single cake of glass or from the same batch. The same cannot be hypothesized for the Trento colorless tesserae, which are compositionally different (Table 2), as detailed in Section 3.1.

In the case of tesserae PN AG1, which was initially interpreted as a silver tessera (from which we derived the label "AG"), the results obtained on the glassy matrix, together the analytical evidence (SEM and XRPD), which shows the absence of silver foil or the residues of any silver compounds, lead us to hypothesize that it is probably a gold tessera, derived from the rim of the cake or an area where the application of the gold foil failed.

The gold foils in the Pordenone samples (PN AU1 and PN AU2) are made of pure gold, while that of TN AU1 is a gold-silver alloy with an Au:Ag ratio of 95:5 (SEM-EDS data); this latter specific composition of the gold foil suggests the use of coins as the source of metal and allows us to hypothesize the dating of the tessera from Trento to the 3rd or 4th century AD [44]. However, given that the mosaic decoration of Trento was destroyed at the beginning of 4th century AD, the dating of this tessera can be restricted to the 3rd century AD.

3.3. Turquoise, Blue and White Tesserae

Samples of the macro groups of turquoise, blue, and white are discussed together because they are mostly characterized by the presence of Ca-antimonates as opacifiers, which are white in color, and are eventually associated with the ionic chromophores as copper and cobalt. The selected tesserae (Table 1—Figure 1b–m) are comprised of 15 turquoise samples (7 from Pordenone and 8 from Trento), 7 blue samples (3 from Pordenone and 4 from Trento) and 5 white samples (2 from Pordenone and 3 from Trento), all opaque, except for 3 translucent tesserae (PN BS1—Figure 1b, TN B1—Figure 1k, and TN BS1), where no opacifier is employed, one semi-opaque (PN-AQ1—Figure 1e) and two banded tesserae (PN TU2—Figure 1c, and PN AZ2—Figure 1l), macroscopically appearing turquoise with black stripes.

Ca-antimonates are present in the form of micrometric euhedral crystals (Figure 3a) that are dispersed in the glassy matrix and are seldom clustered in small lumps. In samples PN TU1, PN TU2, PN AZ2, TN BO1, TN BIOP1 and TN GR1, the distribution of the crystals is uneven (Figure 3b); PN TU2 and PN AZ2, in particular, are banded, with strips of opaque glass in a translucent matrix (Figure 3c). In the other tesserae with Ca-antimonates, crystals are homogeneously distributed into glassy matrix (Figure 3d). Lumps of newly formed crystals are present in all the samples; lumps of partly reacted Ca-antimonate surrounded by newly formed crystals (Figure 3e) and rosary-shaped aggregates (Figure 3f) are also frequent (as in PN TU1, PN TU2, PN TU3, PN CE1, PN GR1, TN TU2, TN TU3, TN CE1, TN BIOP1 and TN VCH1), and this can be indicative of a different production technology that will be discussed later.

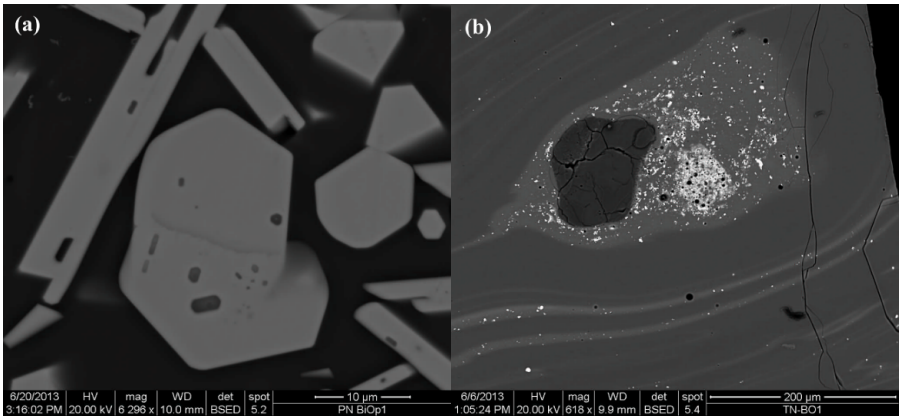

Figure 3. *Cont.*

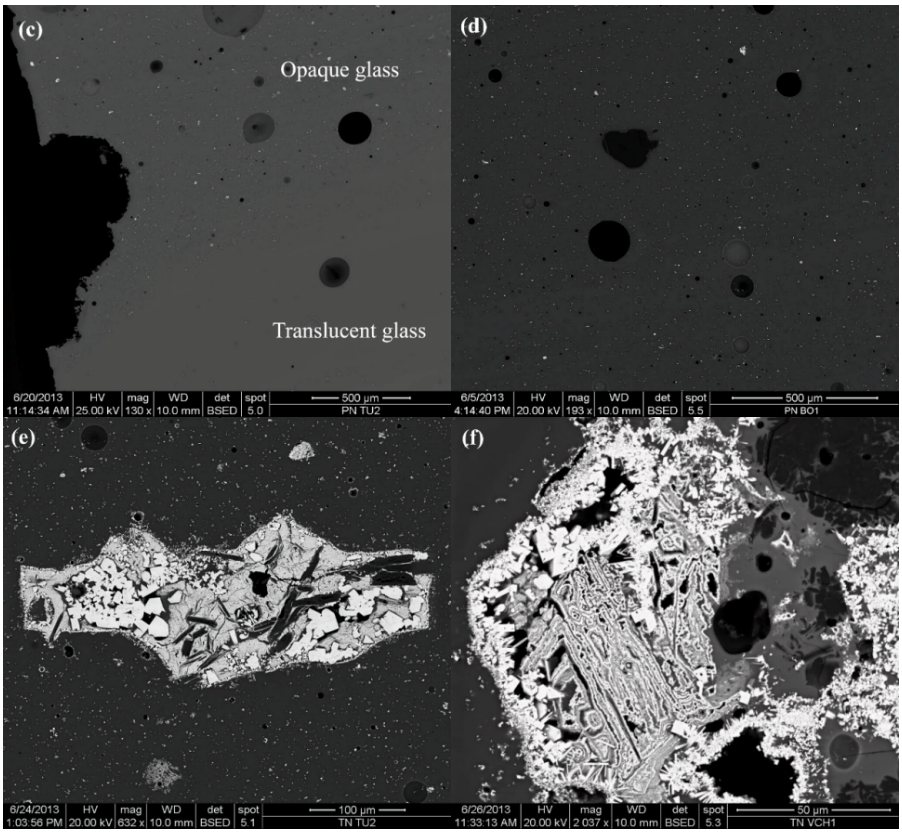

Figure 3. SEM-BSE images of the Ca-antimonate opacified tesserae showing: (**a**) morphology of the Ca-antimonate crystals (tessera PN BIOP1); (**b**) uneven distribution of Ca-antimonates (TN BO1); (**c**) banded micro-texture composed of strips of opaque glass in a translucent matrix (PN TU2); (**d**) homogenous distribution of Ca-antimonates in glassy matrix (PN BO1); (**e**) lump of partly reacted Ca-antimonate associated with newly formed crystals (TN TU2); (**f**) lump of Ca-antimonates with areas characterized by "rosary shaped" aggregation surrounded by larger euhedral crystals (TN VCH1). Grey inclusions in (**b**) and (**d**) are quartz grains.

Furthermore, in the sample PN AQ1 (semi-opaque), rare Ca-antimonates are found in association with very abundant sand relics and gas bubbles. In general, sporadic relics of quartz and feldspars are frequently identified in the glass tesserae, but in the present case, the high relative abundance of such relics and gas bubbles, the sporadic presence of Ca-antimonates and the semi-opaque appearance of the tesserae suggest that quartz sand and gas bubbles may be intentionally involved in the opacity. Such an uncommon micro-textural feature, different from the addition of ground quartz as identified in Medieval mosaics [45], was already identified in a late-Roman glass mosaic from northeastern Italy [30], suggesting that these features may be due to a specific opacification technique. In the archaeometric literature, the scarcity of tesserae with such features may indicate an effective rarity of this technique; however, the identification of the quartz sand relics and gas bubbles is possible only by means of micro-textural characterization of the tesserae, which was not always conducted in the past decades, and future micro-textural studies will shed light on this point.

XRPD analyses, which are performed on the whole tesserae, gave diffraction patterns only on the samples PN TU1, PN TU3, PN CE1, PN AZ1, PN BO1, PN BIOP1, PN GR1, TN TU1, TN AZ2 and TN VCH1; in the other samples, the mineralogical identifications of opacifiers were checked by means of micro-Raman spectroscopy. Taking into account that calcium antimonate has two phases, hexagonal ($CaSb_2O_6$) and rhombic ($Ca_2Sb_2O_7$), the present results show that the association of two phases, with a general prevalence of the hexagonal one, is detected in the majority of tesserae from Trento and Pordenone. Exceptions are the samples PN BIOP1, PN TU1, TN TU1, PN AZ2, TN AZ1,

TN AZ2, TN CE1, TN TU2, which show the hexagonal phase, and the sample PN AZ1, where the rhombic phase is only detected (Figures 4 and 5).

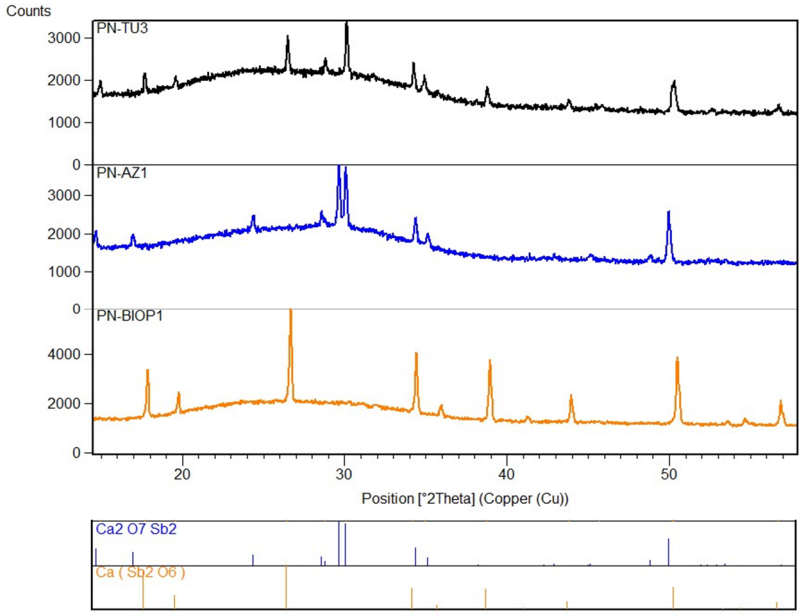

Figure 4. XRPD patterns of tesserae opacified by Ca-antimonates; note the association of the rhombic ($Ca_2Sb_2O_7$) and hexagonal phases ($CaSb_2O_6$) in PN-TU3 (similar pattern in PN CE1, PN BO1, PN GR1, and TN VCH1), and the presence of the only rhombic phase in PN-AZ1, and of the only hexagonal one in PN-BIOP1 (similar pattern in PN TU1, TN TU1 and TN AZ2).

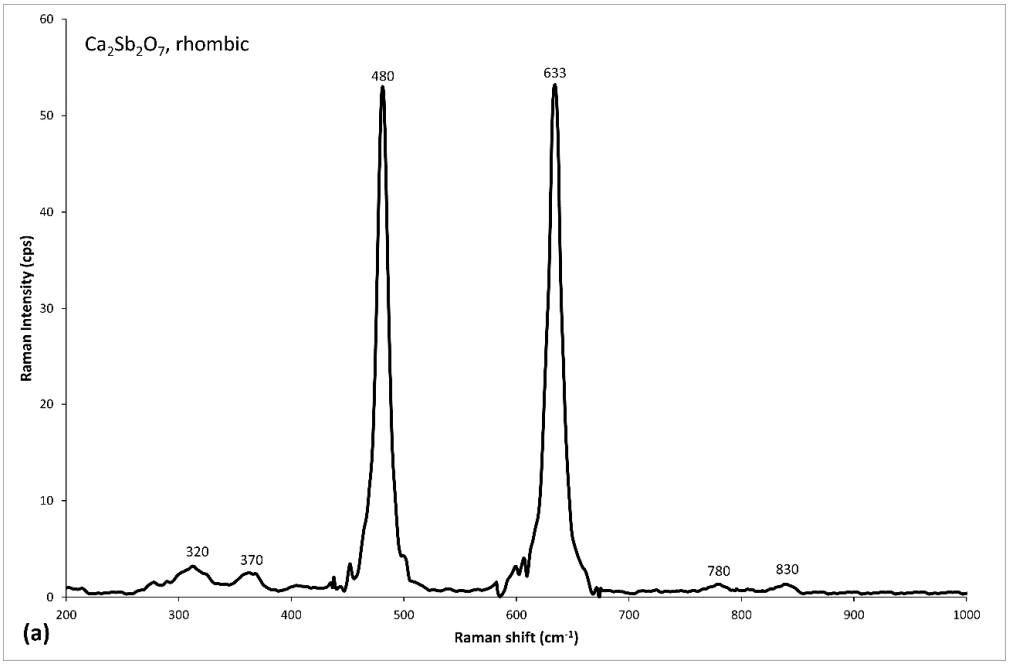

Figure 5. *Cont.*

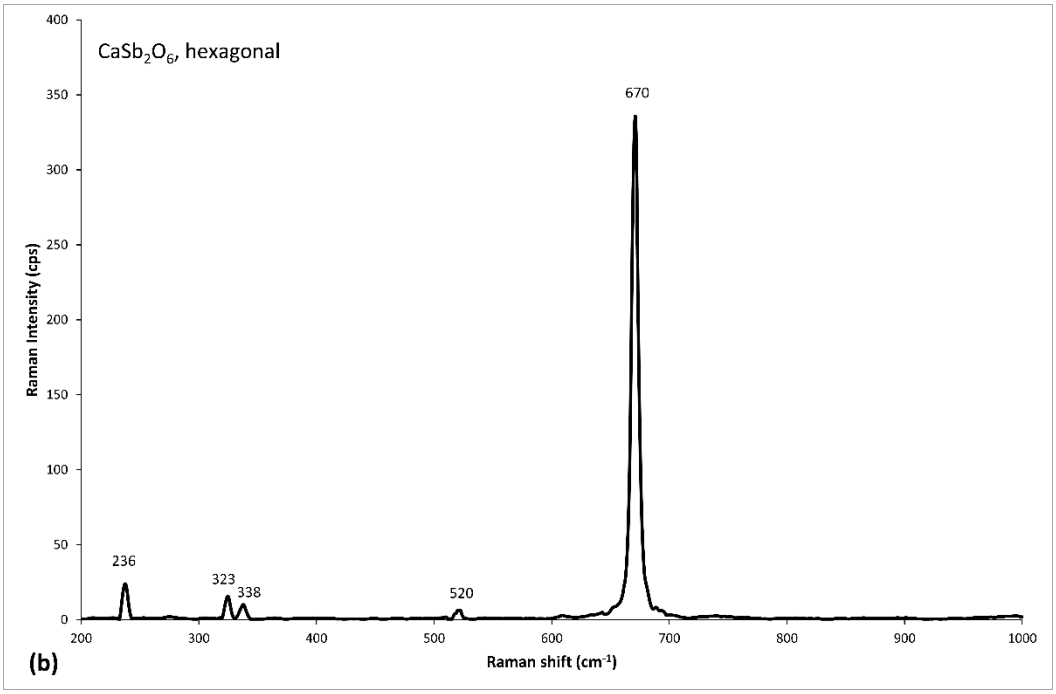

Figure 5. Raman spectra, in the region from 200 to 1000 cm^{-1}, of Ca-antimonates identified in tessera TN TU3: note the presence of measured wavenumbers at 320, 370, **480**, **633**, 780, 830 cm^{-1} for $CaSb_2O_7$ (**a**) and at 236, 323, 338, 520, **670** cm^{-1} for $Ca_2Sb_2O_6$ (**b**) (most intense signals in bold; reference spectra from [46,47]). Both phases, with a prevalence of the hexagonal one, are also detected in TN AQ1, TN AQ2, PN TU2, TN BO1, TN BIOP1, TN GR1, TN GR2, PN VCH1; the hexagonal phase is only detected in PN AZ2, TN AZ1, TN AZ2, TN TU2 and TN CE1.

In regard to the production methods of Ca-antimonate in Roman glass, which hypothesize both *in situ* and *ex situ* crystallization [18], the present micro-textural features, such as the uneven distribution of crystals and the presence of relics of Ca-antimonate and rosary-shaped aggregates suggest that the *ex situ* method was used in PN TU1, PN TU2, PN TU3, PN CE1, PN AZ2, PN GR1, TN TU2, TN TU3, TN CE1, TN BO1, TN BIOP1, TN GR1 and TN VCH1. The same micro-structure was identified in Egyptian white, blue and turquoise opaque glass samples of the 18th Dynasty, for which *ex situ* crystallization is documented [48], although only rhombic phase was detected and not the only hexagonal one or a prevalence of it, as for the present assemblages. For the other tesserae from Pordenone and Trento with Ca-antimonate, showing euhedral crystals finely dispersed in the glass matrix (TN TU1, TN AQ1, TN AQ2, PN BO1, PN AZ1, TN AZ1, TN AZ2, PN BIOP1, TN GR2, PN VCH1), the hypothesis of *in situ* crystallization is more reliable. In previous studies on Roman glass tesserae the *in situ* crystallization is the opacification process, preferentially identified for the production of Ca-antimonate [19], while the present results show that both methods are used, and no relationships between production method and color or site are noted.

In the case of *in situ* crystallization, the occurrence of hexagonal or rhombic phases may be indicative of different firing times and temperatures: the synthesis of pure crystals of Ca-antimonate shows that $CaSb_2O_6$ crystallizes from 927 °C at the expense of $Ca_2Sb_2O_7$, which forms at lower temperatures, and becomes the only phase from 1094 °C [18]. In addition, an experimental study on syntheses of *in situ* Ca-antimonate opacified glass carried out at 1100 °C from periods ranging from 30 min to 13 days, highlights that $CaSb_2O_6$ is kinetically favored, whereas $Ca_2Sb_2O_7$ is thermodynamically stable [19]. Therefore, the presence of both phases, with a prevalence of the hexagonal one, in samples TN AQ1, TN AQ2, PN VCH1, PN BO1 and TN GR2 suggests a firing time of 1–2 days and a temperature of approximately 1100 °C, while the presence of only the hexagonal phase

in TN TU1, TN AZ1, TN AZ2, and PN BIOP1, indicates shorter firing times and higher temperatures (over 1100 °C). Sample PN AZ1, where only the rhombic phase is detected, was probably produced with longer firing times (over two days) and a lower temperature (<1100 °C). Interesting also to note that all the tesserae from Trento and Pordenone with Ca-antimonate, in which the *in situ* crystallization is hypothesized, show a glassy matrix comparable with Mn-glass type. The Mn-glass contains the highest proportion of calcium of Roman glass, making them intrinsically suitable for producing opaque glass, because calcium is conductive to the formation of the calcium antimonate opacifier [12]. In addition, the prevalence of $CaSb_2O_6$ in Trento and Pordenone tesserae may be also facilitated by the low lead content of glassy matrix (Table 2), because this element could stimulate the crystallization of $Ca_2Sb_2O_7$, as already observed in previous studies on Roman and modern opaque glass with high lead contents (from 2 to 25 wt % as PbO) [19].

In regard to the cause of color, in the turquoise color macro-group, the ionic colorant is copper, probably in its oxidized state (Cu^{2+}). The average concentration of copper in this group reaches almost 3 wt % as CuO, with a maximum value of approximately 5 wt % (Table 2). Copper-colored tesserae always contain some tin (an average of 0.17 wt % as SnO_2), and three analytical samples from Pordenone (corresponding to two tesserae, PN TU2 and PN TU3) also contain some zinc (approximately 0.10 wt % as ZnO in both tesserae—Table 2), which might be indicative of the use of metalworking scraps, such as bronze and brass, as the source of copper [49], although the possible contemporary use of copper minerals cannot be excluded due to the presence of sporadic drops of copper sulfide, which was identified by means of SEM-EDS analyses.

In the blue macro-group, the ionic colorant is cobalt, which is below 0.2 wt % as CoO (Table 2). In the case of the azure tessera TN AZ1, where the concentration of cobalt appears below the detection limits of EPMA (i.e., <0.03 wt % as CoO, Table 2), this chromophoric ion was checked by means of FORS spectrometry (Figure 6). Cobalt colored tesserae contain also copper in a low concentration (below 0.60 wt % as CuO) and a relatively high iron oxide concentration (up to 1.89 wt % as Fe_2O_3—Table 2), and, although good linear correlations are missing, copper and iron show a somewhat positive trend with cobalt, suggesting that these elements may derive from the cobalt ore or from the same mineralogical association [50,51].

In the white macro-group, the color and opacity are given only by the opacifiers in the white sample while, in the case of the gray samples, a very weak signal of cobalt was detected by means of FORS spectrometry (Figure 6), suggesting that the gray color is due to the combination of a very pale blue tinge, due to cobalt, and the white color of the opacifiers.

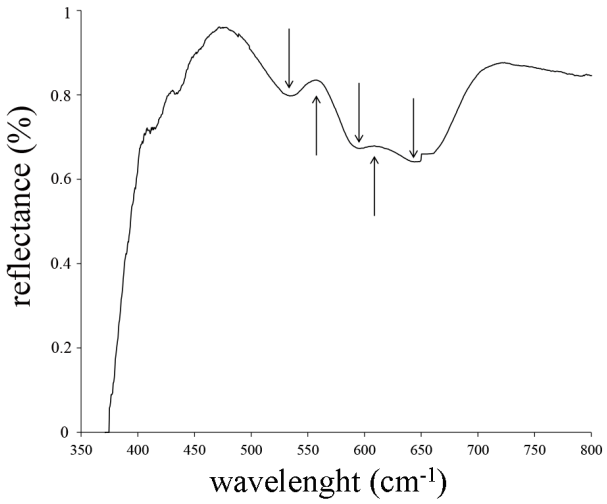

Figure 6. FORS spectrum of the azure tessera TN AZ1, showing maximum reflectance at 550 and 625 nm and a minimum of reflectance at 525, 600 and 650 nm [52], in accordance with the presence of cobalt in the visible interval. Similar spectra are obtained for grey tesserae.

3.4. Yellow and Green Tesserae

Samples of the macro groups yellow and green are mostly characterized by Pb-antimonate as the opacifier, which is yellow in color. The selected tesserae (Table 1–Figure 1n–t) are composed of eight yellow (four from Pordenone and four from Trento) and nine green samples (four from Pordenone and five from Trento) and are further subdivided into various colors as described in section on "Materials." All the selected tesserae are opaque or semi-opaque, except for one translucent yellow (TN VG2—Figure 1r) and four translucent green (PN VTR1—Figure 1o, PN VTR2, TN VS1, TN VOL2—Figure 1q) tesserae, where no opacifier is employed.

Pb-antimonate is present in the form of micrometric crystals or in clusters with anhedral or subhedral habitus (Figure 7a,b) and is distributed in the glassy matrices in non-homogenous textures, which are often concentrated in bands and clustered in lumps; the glassy matrix of these samples is zoned, with the bands of higher average atomic number visible in the BSE images, due to different contents of heavy elements, lead in particular (Figure 7c). In tessera TN VG1, which is semiopaque, very rare opacifiers are coupled with many gas bubbles, that contribute to increase opacity (Figure 7d). In PN GSO2, the banding due to very different lead contents and uneven distribution of opacifier, clearly evident in SEM-BSE images, is also visible to the naked eye as a few strips of well-opacified yellow glass alternating with semi-opaque or transparent areas (Figure 8).

In the yellow (GSO) and light amber (NC) samples, the opacifiers are embedded in a colorless glassy matrix, while in the yellow-green (VG), green (VP) and dark green (VS) ones, they are dispersed in a glassy matrix colored by copper and, eventually, iron.

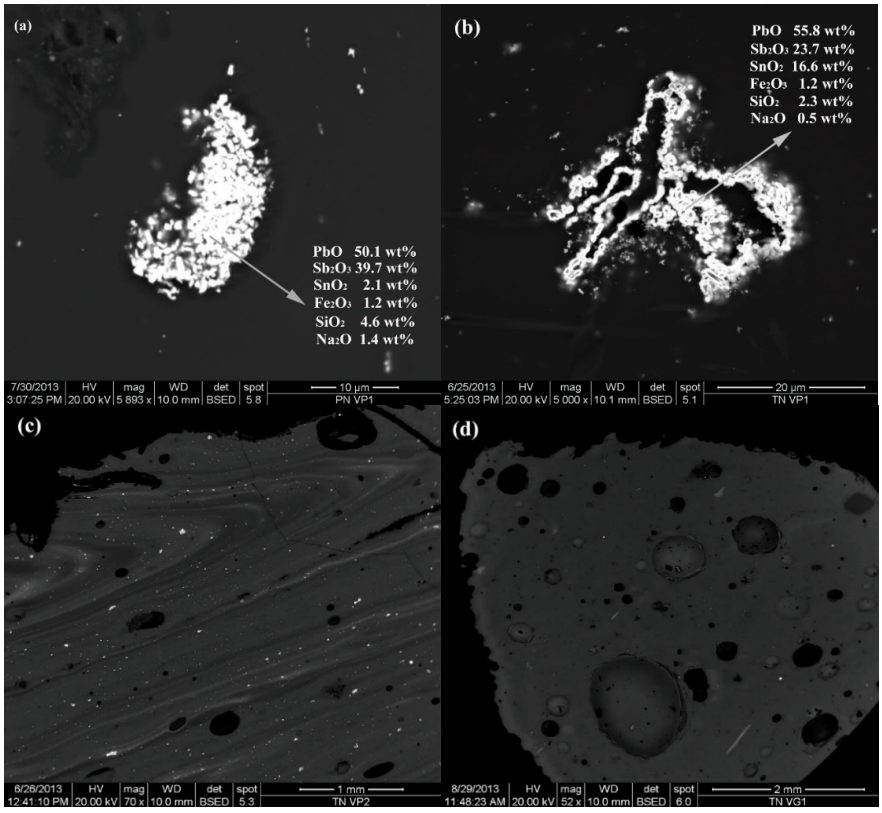

Figure 7. SEM-BSE images of Pb-antimonate opacified tesserae showing: (**a**) subhedral habit of Pb-antimonate (tessera PN VP1); (**b**) anhedral habit of Pb-antimonate (TN VP1); (**c**,**d**) various micro-textures of the glassy matrix shown by Pb-antimonate opacified tesserae (TNVP2 in (**c**) and TN VG1 in (**d**)). Note bands with different average atomic numbers and uneven distribution of opacifier in (**c**), and rare opacifiers coupled with many gas bubbles in (**d**). Chemical compositions of opacifier also reported in (**a**) and (**b**) (SEM-EDS data).

EDS qualitative analyses on the crystals highlight the presence of lead and antimony, which are associated with other elements, such as sodium, silicon and iron. While silicon and sodium are seldom detected and belong to the glassy matrix, iron (mean content of approximately 1.5 wt % and up to 3.5 wt % as Fe_2O_3—SEM-EDS data) is present in every analyzed crystal and is more probably pertinent to the opacifiers [49]. The majority of the inclusions also contain tin, which is present in variable concentrations from crystal to crystal and from sample to sample, but, in any case, the tin content is always lower than the antimony content. In particular, the opacifiers in PN GSO1, PN VG1, PN NC1, PN VP1, PN VS1, TN GSO2, TN VG1, TN VP2 and TN VS2 have a tin content that varies from non-detectable to approximately 5% as SnO_2, while those in PN GSO2, TN GSO1 and TN VP1 have a higher tin content, ranging from 11 to 16 wt % as SnO_2 (SEM-EDS data; Figure 7a,b and Figure 8d).

For a more precise identification of the phase used as opacifier in the yellow and green tesserae from Pordenone and Trento, a combination of techniques (SEM-EDS, XRPD and/or micro-Raman spectroscopy) is here carried out.

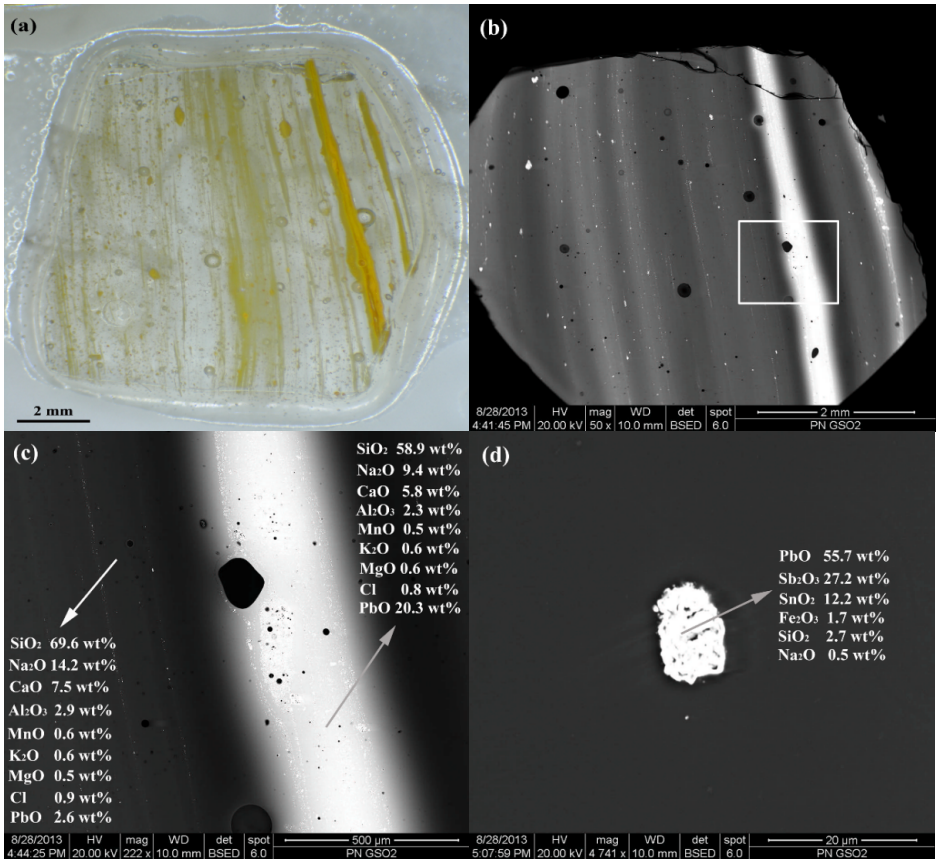

Figure 8. OM (**a**) and SEM-BSE (**b**–**d**) images of tessera PN GSO2, opacified with Pb-antimonate. Note banding (**a**–**c**), and anhedral habit of Pb-antimonate (**d**). Chemical compositions of bands and opacifier also reported in (**c**) and (**d**), respectively (SEM-EDS data). Black inclusions in (**c**) are quartz grains.

XRPD identified a cubic pyrochlore that is similar to Pb-antimonate ($Pb_2Sb_2O_7$), but with a certain degree of substitution, in samples PN GSO1, PN VP1, PN VG1, TN VS2, TN GSO1, TN GSO2, TN VP1 and TN VP2 (in the other samples, the opacifiers were only checked by means of SEM-EDS and micro-Raman spectroscopy). Unfortunately, this analytical technique did not allow the precise crystallographic identification of the phase. Cubic pyrochlores of tin, antimony and lead, in fact, constitute a solid solution between the two end members: that with only antimony and lead (Pb-antimonate) and that with only tin and lead (Pb-stannate). This is reflected in the remarkable

chemical variability of the crystals, shown by SEM-EDS analyses, which further complicates the exact identification by means of XRPD. For this reason, from the XRPD viewpoint (Figure 9), the phases identified in the present assemblage are better interpreted as generic synthetic pyrochlores of the kind $Pb_2MSbO_{6.5}$ (M = Ti, Zr, Sn, Hf) [53]. The micro-Raman spectra of opacifiers used in green and yellow tesserae from Pordenone and Trento show the typical features assigned to lead-tin antimonate, in good agreement with the literature [47,54,55]: an intense peak at 140 cm^{-1}, due to stretching vibration of Pb–O, and various bands at 330, 450 and 510 cm^{-1}, involving the more covalent and rigid Sb–O bonds, which change when the Pb-antimonate structure is distorted by the insertion of a third larger cation, as Sn^{4+} replacing Sb^{5+}. The shift towards higher wavenumbers of the Pb–O lattice mode (from 110 to about 140 cm^{-1}), and, in particular, the intensity decrease of the band at 510 cm^{-1}, accompanied by the clear increase of a band at about 330 cm^{-1} and the appearance of a weak band at about 450 cm^{-1} are diagnostic markers of Pb-antimonate doped with tin (Figure 10).

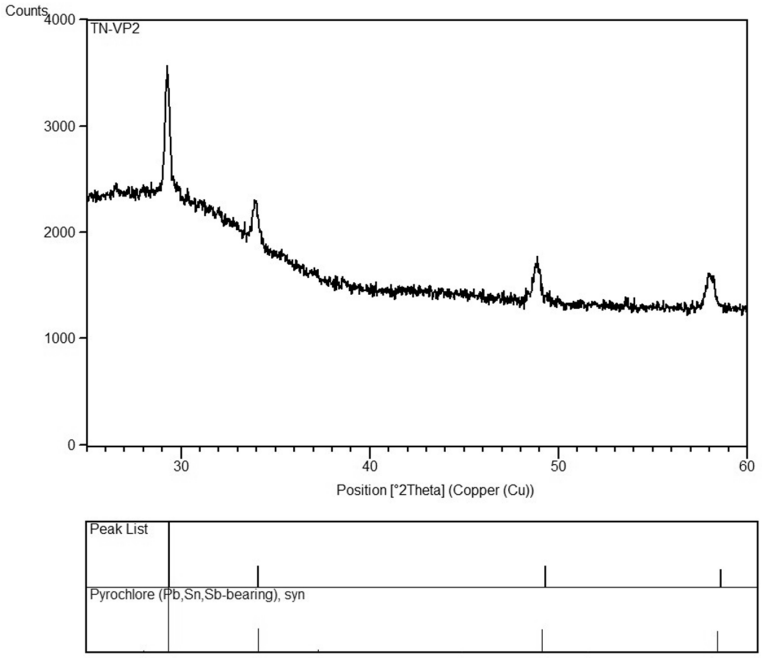

Figure 9. XRPD pattern of tessera TN VP2 opacified by generic synthetic pyrochlores, containing Pb, Sb and Sn. Similar pattern shown by PN GSO1, PN VP1, PN VG1, TN VS2, TN GSO1, TN GSO2, and TN VP1.

Therefore, the combination of results, obtained by means of SEM-EDS, XRPD and micro-Raman spectroscopy, allows us to identify the phase used as opacifier in the yellow and green tesserae from Pordenone and Trento as Pb-antimonates, with variable but generally low tin content, or better as pyrochlores of the kind $Pb_2Sb_{2-x}Sn_xO_{7-x/2}$.

The *ex situ* production method of Pb-antimonate, commonly accepted in the literature for this kind of opacifiers [17,18], is consistent with the uneven distribution of crystals observed in the tesserae investigated here. Tin-rich Pb-antimonate are testified in the literature both in glass [17,20,56,57], where they are interpreted as Pb-antimonates, and in painting pigments, classified as "triple oxides of Sn, Pb and Sb" [58,59]. Many hypotheses were advanced to explain the presence of tin in Pb-antimonate [17,18]. In the present assemblage, given the high tin detected in the opacifiers of some tesserae analyzed here, the most likely hypotheses are the use of tin-rich metallurgical scraps as the source of lead or the intentional addition of it as a stabilizer [17]; it is unlikely that this element is a pollutant *s.s.* The occasional presence of iron in the crystals, which was already detected in Roman and Byzantine yellow glasses [9,17,18], is also of unclear origin, and pollution or a deliberate addition [17] are both reliable hypotheses. In addition, as can be observed in Figure 10, the collapse of the peak at

about 200 cm^{-1}, the strengthening of the band at 330 cm^{-1} and the broadening of that at 510 cm^{-1} suggest firing temperatures of about 900–1000 °C for the production of Pb-antimonate [55].

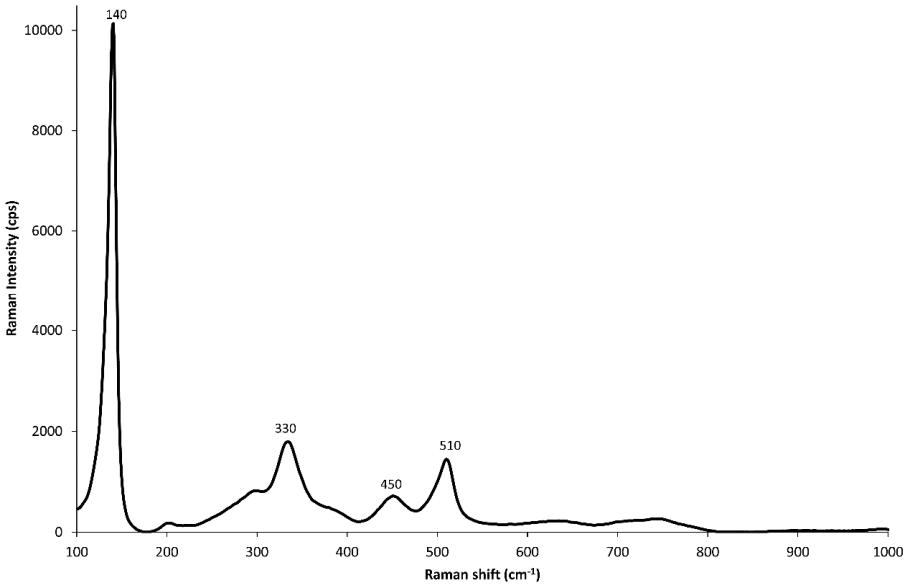

Figure 10. Raman spectrum, in the region from 100 to 1000 cm^{-1}, of opacifier identified in tessera PN GSO2: note the presence of measured wavenumbers at **140**, 330, 450, 510 typical of Pb-antimonate doped with tin (most intense signal in bold; reference spectra from [47,54,55]). Similar spectra are identified in TN VG1, PN NC1, PN VS1, PN GSO1 and TN VP1.

Four tesserae included in the green macro-group are translucent: an olive-green tessera (TN VOL2) and three translucent dark green tesserae (PN VTR1, PN VTR2 and TN VS1). Olive green is a very common tint in naturally colored Roman and late Roman glass vessels (for instance, HIMT glass [60]), mostly due to the iron oxide that is naturally present in sand; in the case of tessera TN VOL2, however, the very high iron content (2.46 wt % as Fe_2O_3) is coupled with very high copper (2.07 wt % as CuO), which is also probably involved in the coloring; in addition, the presence of lead, antimony and tin (Table 2) is surely not related to the opacifiers, which are absent here, and it suggests that this sample is linked to the production of red glass. Therefore, any further discussion is reported in the sub-section on "red tesserae".

The tesserae PN VTR1 (Figure 1o), PN VTR2 and TN VS1 show a strong emerald green color. This color, also named "peacock green" [61], is relatively rare in ancient glassmaking and is characteristic of the early Roman production of luxurious, deeply colored vessels; this kind of glass is usually characterized by the use of plant-ash based glass and copper oxide as a chromophore [12,34,61,62]. In the emerald green tesserae investigated here, the base glass employed is unequivocally natron-based, but, despite the apparent chromatic similarity among the three samples, a major compositional difference emerges (Table 2): in the case of TN VS1, copper is the colorant ion (1.84 wt % as CuO), while in the case of PN VTR1 and PN VTR2, the only colorant ion detected is iron (1.92 and 2.79 wt % as Fe_2O_3, respectively). This was also confirmed by EPR analysis, which excluded the presence of copper and measured iron as Fe^{2+} and Fe^{3+} with a neat prevalence of Fe^{3+} (Figure 11) in both PN VTR1 and PN VTR2. While the copper-based coloring technique employed in Trento is quite common, the two samples from Pordenone, both iron-colored, were produced using a technique that is rare in mosaic tesserae and was previously identified in one early Roman tessera (see sample 18 from West Clacton Reservoir [12,61]); such evidence reinforces the hypothesis of early Roman dating for the assemblage from Pordenone. The translucent emerald green samples analyzed here are a testament to the diversity of technological choices that were applied in ancient Roman glassmaking to obtain the same color.

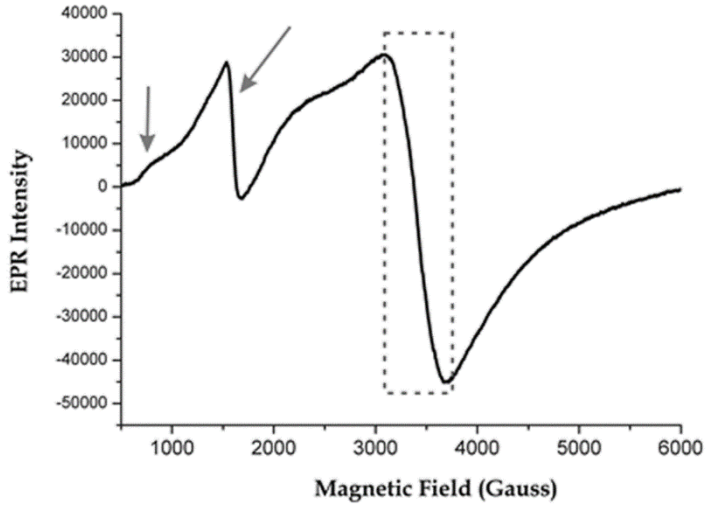

Figure 11. EPR spectrum of sample PN VTR1, equivalent to that of PN VTR2. The arrows highlight the signal of Fe^{3+} while the dotted area highlights a shoulder referable to Mn^{2+} No signal referable to copper was identified.

3.5. Red Tesserae

The red macro-group comprises eight tesserae (four from Pordenone and four from Trento—Table 1—Figure 1u–x) of various shades of brown (M) and orange (AV) that are colored and opacified by means of copper phases; in addition, two green/red striped (PN M3 and TN VOL1—Figure 1y) and one dark amber (TN NS1—Figure 1z) tesserae are also included here, due to their textural and technological characteristics, which are closer to the red samples than to the other macro-groups.

In the brown tesserae, the color ranges from red to almost black, and, apart from one homogenous sample (TN M3), all the others are banded with areas of darker and brighter color (Figure 1u,v); the orange samples comprise a single homogenous tessera, i.e., PN AV1 and two (PN AV2 and TN AV1) with bands that are orange and bright red in color (Figure 1w–x).

Micro-textural examination of the brown samples highlighted the presence of abundant nanometric crystals (≈100 nm) of cubic habitus (Figure 12a); in the orange ones, very abundant nanometric-to-micrometric crystals of rounded/elongated habitus, were identified (Figure 12b). In the case of the green/red striped tesserae, the nanometric cubic crystals are concentrated in the red stripes (Figure 12c,d), while, in the dark amber, they are rare but well distributed.

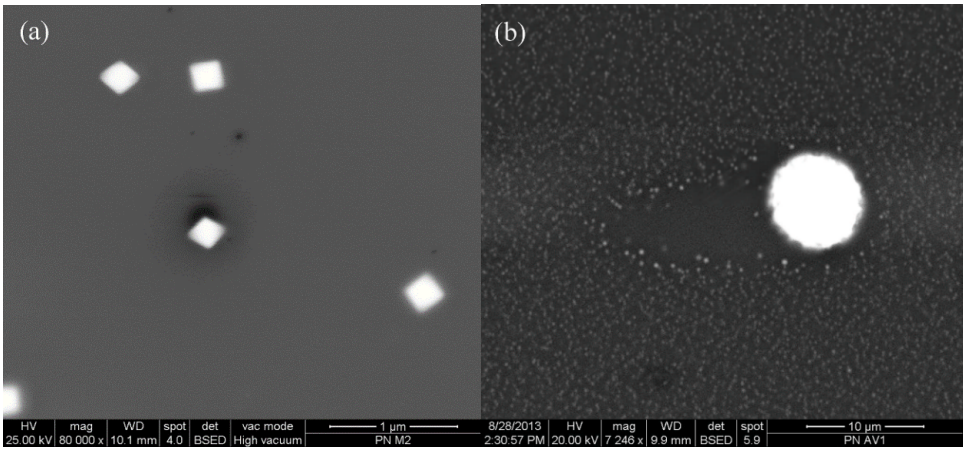

Figure 12. *Cont.*

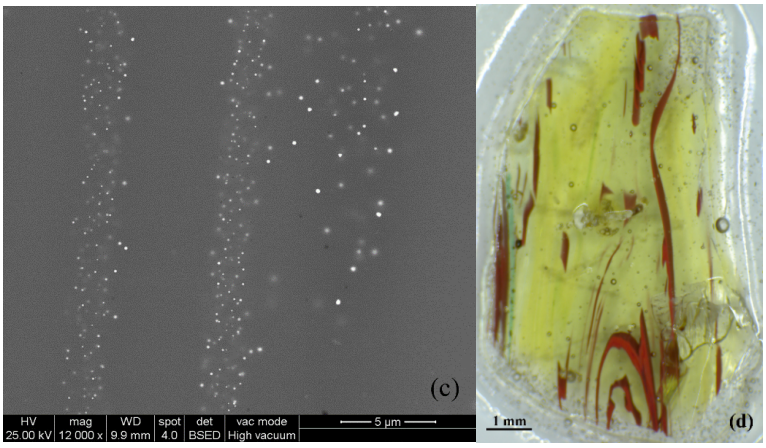

Figure 12. SEM-BSE (**a**–**c**) and OM (**d**) images of the copper-phases opacified tesserae showing (**a**) euhedral cubic nanocrystals of metallic copper (tessera PN M2); (**b**) sub-rounded crystals of cuprite (PN AV1); the bright drop is metallic copper; (**c**,**d**) micro-texture of green/red tessera PN M3 characterized by metallic copper crystals in opaque red stripes and absence of opacifier in translucent green stripes.

XRPD and micro-XRD analyses confirmed the presence of metallic copper in the brown TN M1, TN M2 and TN M3 and the presence of cuprite in all the orange samples, including the red stripes of the orange/red-banded tesserae PN AV2 and TN AV1 (Figure 13); the brown samples from Pordenone (PN M1 and PN M2), the green/red striped PN M3 and TN VOL1 and the dark amber TN NS1 sample did not give any diffraction patterns, which is probably due to the low frequency and/or the low crystallinity degree of the inclusions; however, the chromatic appearance of the above tesserae (i.e., the dark hue of red), and the SEM-EDS data, combined with the chemical compositions of the glassy matrix characterized by low contents of copper and lead (Table 2), suggest that metallic copper is the phase involved in the coloring, as already identified in red tesserae with similar color, micro-texture and chemical composition [4,8,10,11,15,22,63].

Despite their similarity in terms of color and chemical composition, the banded pattern that characterizes the brown tesserae has different chemical and textural explanations. In the brown-banded samples from Trento, the darker areas (brighter in the SEM-BSE image—see Figure 14a) correspond to a higher iron oxide content (Table 2, sample TN M2 (dark)) and to a higher relative abundance of large crystals that reach micrometric size (Figure 14b); in the Pordenone samples, the macroscopic banding is related to different chemical or micro-textural features. In PN M1, the non-homogeneity of glassy matrix visible in SEM-BSE images (Figure 14c) and confirmed by EDS data, which show high lead, iron and copper in brighter areas and low lead, iron and copper in darker areas, has strict connection with the macroscopic banding; for instance, the large black band at the center of the sample, which appears partly translucent and greenish when examined in OM (Figure 14d), corresponds to darker area of SEM-BSE image, suggesting that the macroscopic banding might be due to different compositions of glassy matrix. In the case of PN M2, the different stripes have no link with the glassy matrix composition, which is indeed quite homogeneous; BSE image (Figure 14e) shows a micro-texture composed of bands with many crystals alternating with apparently clear bands that have no opacifier and also macroscopically, the stripes appear both opaque red and translucent greenish (Figure 14f). This suggests that in PN M2 the macro-banding is due to different micro-textural distributions of opacifier. In addition, the various hues of opaque red stripes may be related to different dimensions of opacifiers, which are larger in darker red bands.

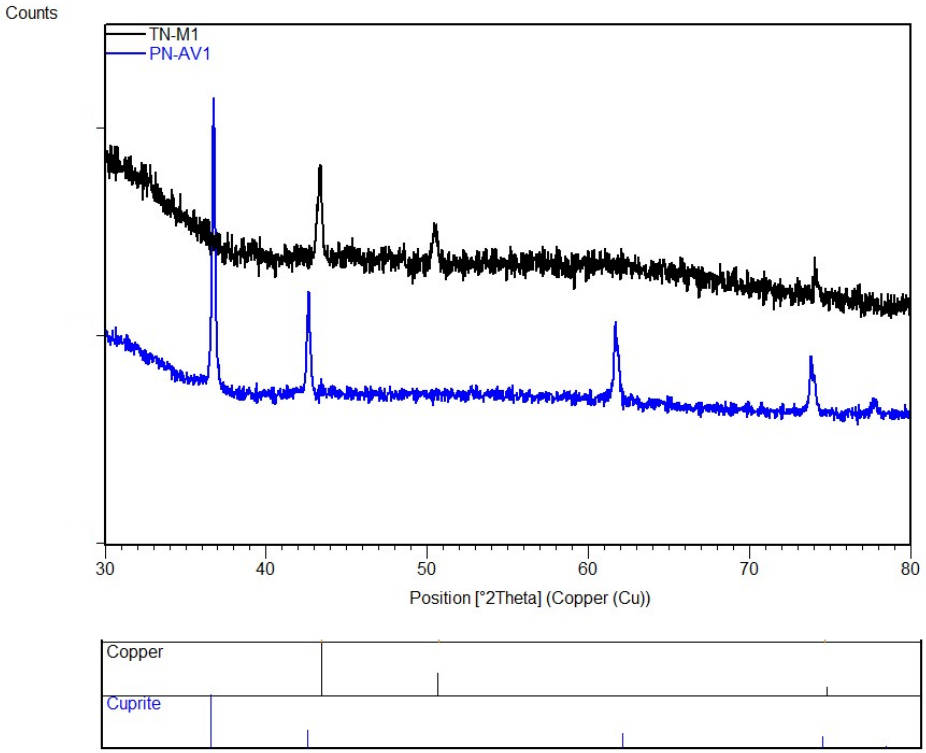

Figure 13. XRPD patterns of tesserae opacified by copper phases; note the presence of metallic copper in TN-M1 (black line; similar pattern shown by TN M2 and TN M3) and of cuprite in PN-AV1 (blue line; similar pattern shown by PN-AV2 and TN AV1).

In the orange/red-banded samples (TN AV1 and PN AV2), the bi-colored pattern also has different explanations: TN AV1 shows a homogenous glassy matrix of low average atomic number, where abundant bright crystals are embedded; areas of larger crystals, seldom clustered in small lumps, correspond to red stripes, while areas with smaller and denser crystals correspond to orange stripes (Figure 14g,h). In sample PN AV2, conversely, the glassy matrix is chemically non-homogenous, with stripes of different atomic number, which resemble the pattern visible by OM, suggesting that the red/orange banding is due to different chemical compositions of glassy matrix, being the red stripes enriched in lead with respect to the orange ones (Figure 14i,j).

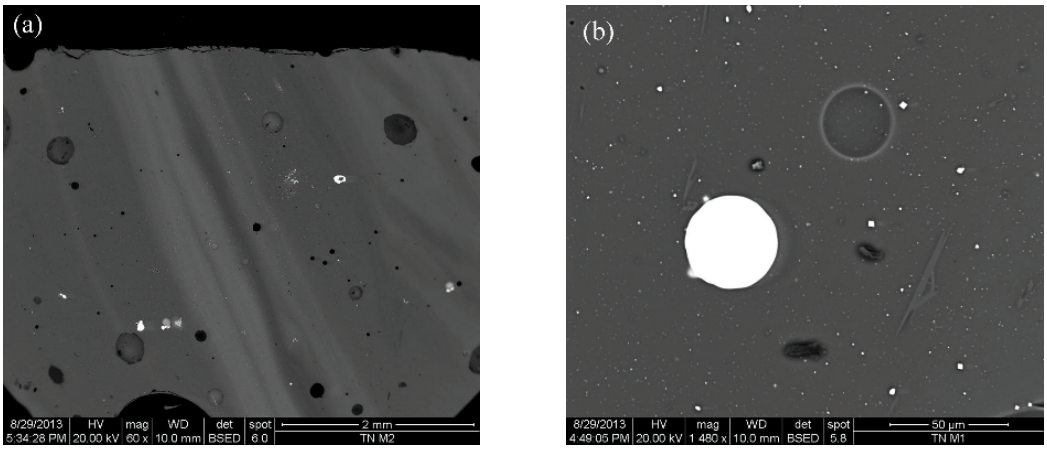

Figure 14. *Cont.*

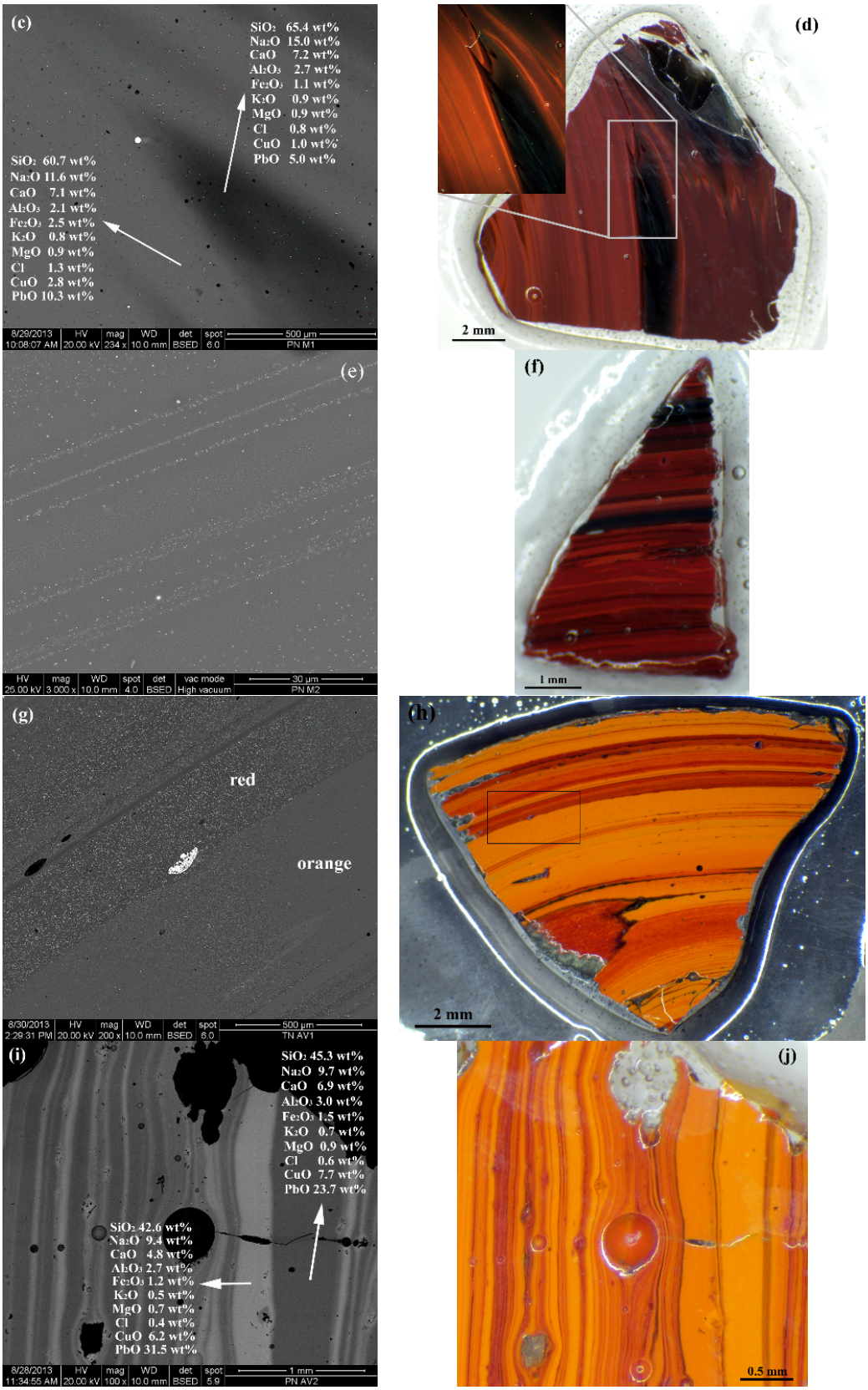

Figure 14. SEM-BSE (**a**–**c**,**e**,**g**,**i**) and OM (**d**,**f**,**h**,**j**) images of various micro-textures of red-banded tesserae: (**a**) TN M2: the banding is due to a variable concentration of iron, which is higher in brighter areas, and relative abundance of crystals; white inclusions are iron oxides. (**b**) TN M1: metallic copper crystals of micrometric and nanometric size are visible; the white rounded drop is a segregation of metallic copper;

(**c**,**d**) PN M1: note that the banding is due to different compositions of glassy matrix, with a direct link to macroscopic color (SEM-EDS data also reported in c); (**e**,**f**) PN M2: note bands rich in metallic copper crystals, alternating with clear glassy matrix; micro-texture resembles macroscopic banding composed of opaque red and translucent green bands; (**g**,**h**) TN AV1: note the homogenous glassy matrix and the differences in crystal size related to red and orange bands; (**i**,**j**) PN AV2: non-homogenous glassy matrix due to an uneven lead content, related to the macroscopic red/orange banding (SEM-EDS data also reported in (**i**).

Independently from the causes of banding, it is interesting to note that in other assemblages, the presence of banded tesserae with two colors, each having different chemical compositions and opacifiers, is testified [36], and this strongly supports the deliberate combination of two different kinds of glass to obtain a bi-colored pattern. In the current assemblage, the bi-colored patterns may be also obtained accidentally during the coloring/opacifying step, although their deliberate production cannot be completely excluded.

Apart from the textural and compositional differences, which were described previously, the brown and orange samples from Pordenone and Trento both have a copper-based pigment, which is composed of metallic copper or cuprite, respectively. The production of the red color, which is as ancient as glass itself [64], requires a reducing atmosphere in the furnace and the melt in order to obtain the reduction of copper from Cu^{2+} to Cu^{1+} (in the case of cuprite) or Cu^{0} (in the case of metallic copper). The achievement of local reducing conditions in the melt was aided by internal reducing agents, such as iron, tin and, probably, charcoal or furnace ashes that are rich in carbon residues [44,45]; charcoal and furnace ashes in particular, when added to the glass, introduce carbon and other elements, such as magnesia, potash, or phosphorous oxide, and this might be responsible for the plant-ash fingerprint of some red Roman glasses. The plant-ash appearance of brown tessera PN M1 would be related to the reducing condition of furnace and not to different base-glass. In the other brown samples investigated here that do not present the "plant-ash fingerprint," the role of the reducing agent is played by iron, tin, antimony and lead, which are present in variable amounts (Table 2).

Taking into account the contents of lead and copper in the red samples (including also the tessera TN VOL2—see previous section), a major distinction emerges. As highlighted in Figure 15, and according to the classification of Freestone et al. [15], the samples are split into two main groups: a high copper-high lead group, comprising all the orange tesserae from Pordenone and a low copper-low lead group, comprising all the brown tesserae, green/red TN VOL1, dark amber TN NS1 and olive green TN VOL2. Two samples do not follow the grouping: green/red PN M3, in which the lead content is intermediate between the two groups, and orange/red TN AV1 (both orange and red bands), which has a specific composition with low lead and high copper. It is usually reported in the literature that high lead plays a key role for the development of cuprite in glass [65–68], but in tessera PN AV1 (cuprite colored), the lead level is comparable to that of the brown samples with metallic copper (Figure 15). This evidence suggests that the formation of cuprite, certainly aided by the presence of lead, is also favored by the availability of abundant copper and, in the presence of excess copper, the quantity of lead required for the nucleation of cuprite decreases dramatically.

Finally, green/red striped samples TN VOL1 and PN M3 can be interpreted as "failed" red tesserae. In both cases, diagnostic elements, such as tin, antimony and zinc, are present, and iron is higher with respect to the copper-colored turquoise or green glass and closer to content of red tesserae (Table 2), suggesting that the desired color might be red. A lack of control in the redox-condition probably caused the generation of green/red bands, and the big difference in lead contents (high in PN M3 and low in TN VOL1—Figure 15) supports the hypothesis that lead does not have a key role for the development of metallic copper. Similar conclusions can be drawn for the translucent olive-green sample TN VOL2 (already mentioned in sub-section on green tesserae), whose chemical composition, which is close to that of PN M3, suggests that this tessera may also be the result of a failed attempt to produce red glass, even if, in this case, no red stripe was generated, probably due to unsuitable redox-conditions in furnace.

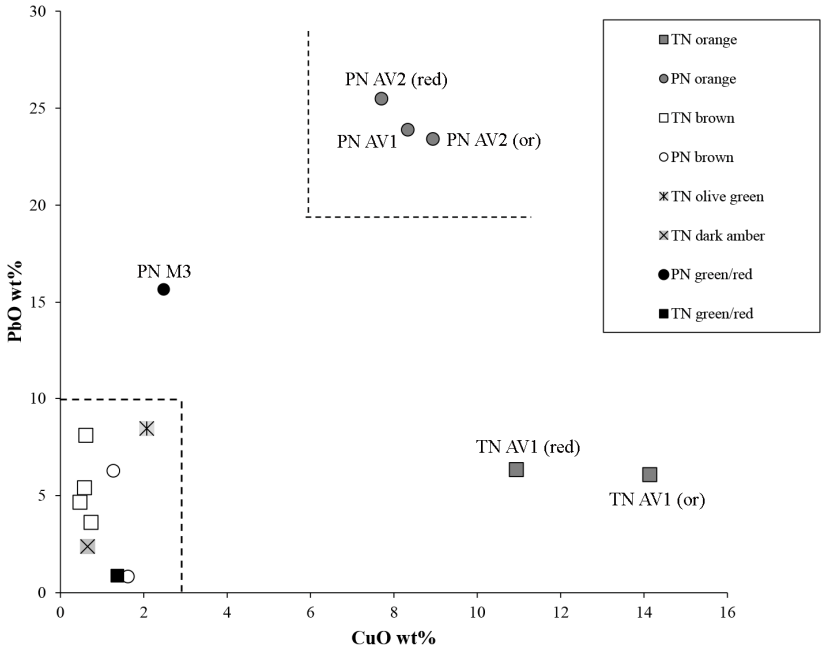

Figure 15. PbO *vs* CuO bi-plot of red tesserae; olive-green tessera TN VOL2 is also included (see text for details). Dotted lines mark the low-copper/low-lead and high-copper/high-lead fields according to Freestone et al. [15].

4. Conclusions

The textural, chemical, mineralogical, and spectroscopic study of glass tesserae from two sites in northeastern Italy, Pordenone and Trento, allowed us to investigate the variety of technological solutions employed in the production of each color during Roman times.

The assemblage investigated here comprises a wide range of colors that are comparable between the two sites. The most common colors are blue, turquoise and green, which are typical of Roman mosaic decorations.

The wide chronological frame considered, in particular for the assemblage from Pordenone, the chemical composition of glassy matrices, and the opacification and coloring techniques employed are comparable to those typical in the Roman centuries; therefore, the production of the tesserae can be traced back to the early Roman times.

Despite the overall homogeneity and a general comparability with published data on glass tesserae coeval in age, some differences in the technological procedures used for obtaining the same color were identified (for instance, the *in situ* or *ex situ* crystallization of Ca-antimonates in white, turquoise and blue tesserae, the presence of different contents of tin in Pb-antimonate crystals in yellow and green tesserae, the use of brass or bronze as the source of copper in turquoise, yellow and green tesserae. Less common coloring and opacification techniques were also identified in two emerald green (iron-colored instead of copper-colored) and one turquoise (opacified by bubbles and quartz relics) tesserae, all from Pordenone, highlighting the variety of the *chaine operatoire* in the production of colored glass in Roman times.

The macro-banded textures, identified in variously colored samples, are not due to the mixing of different colored glasses, as documented in the literature for Byzantine mosaics (e.g., [11,13]). In particular, in the azure, turquoise and yellow banded tesserae (all from Pordenone), the pattern is related to the opacification process, which was likely conducted by adding the opacifier to a barely softened glass in a very quick process, and this practice developed bands of translucent and opaque glass of the same color due to non-homogenous distribution of crystals. In the case of the orange and brown tesserae, where the opacifier is always precipitated *in situ*, the bands of different colors

are due to differences in the crystal size or distribution of opacifier, and/or chemical composition of glassy matrix. Lastly, given the chemical composition of the glassy matrix, the green/red-banded tesserae and the olive-green sample from Trento may be also considered the result of a failed attempt to produce red glass.

In conclusion, independently from the causes of non-homogenous textures, it is interesting to note that the banded tesserae were not discarded by Roman glass-makers, because these textures enhance the chromatic range and improve the "impressionistic" effects of mosaic decoration, and, even though the non-homogenous textures may be considered accidental in the majority of cases studied here, their deliberate production cannot be completely excluded.

Supplementary Materials: The following are available online at http://www.mdpi.com/2075-163X/8/6/255/s1, Table S1: EPMA analytical conditions, Table S2: Comparisons between "known" values and data from EPMA for standard glass "Corning B".

Author Contributions: S.M. performed sampling and analyses; A.S. contributed to the interpretation of analytical data and to the conception of the work. Both the authors read and approved the submitted manuscript, and agree to be personally accountable for the own contributions and for ensuring that questions related to the accuracy and integrity of any part of the work, even ones in which they were not personally involved, are appropriately investigated, resolved and documented in the literature.

Acknowledgments: The authors are grateful to the *Soprintendenza Archeologia, Belle Arti e Paesaggio del Friuli Venezia Giulia* and the *Soprintendenza per i Beni Architettonici e Archeologici-Ufficio Beni Archeologici della Provincia Autonoma di Trento* for authorising the present study; AnnaNicoletta Rigoni (*Museo Archeologico del Friuli Occidentale*) and Maria Teresa Guaitoli (*Alma Mater Studiorum-Università degli Studi di Bologna*) for providing the samples and for their archaeological support; Mariangela Vandini, Tania Chinni (Alma Mater Studiorum-Università degli Studi di Bologna) and Paolo Guerriero (CNR-ICMATE) for the collaboration in SEM-EDS analyses; Raul Carampin (CNR-IGG) for EPMA analysis; Federico Zorzi and Fabrizio Nestola for XRD analyses; Alfonso Zoleo for FORS and EPR measurements. Gianmario Molin is also thanked for useful discussion. Financial support was provided by the project "PRAT 2012" of the University of Padova, named "Crystals in ancient glass mosaics as indicators of raw materials and production technologies" (grant number: CPDA127550). The authors are grateful to anonymous referees for their constructive review of this manuscript.

Conflicts of Interest: The authors declare no conflict of interest.

References

1. Verità, M. Tecniche di fabbricazione dei materiali musivi vitrei. Indagini chimiche e mineralogiche. In *Medieval Mosaics Light, Color, Materials*; Borsook, E., Gioffredi Superbi, F., Pagliarulo, G., Eds.; Silvana Editoriale S.p.A.: Cinisello Balsamo, Italy, 2000; pp. 47–64, ISBN 88-8215-265-0.
2. Galli, S.; Mastelloni, M.; Ponterio, R.; Sabatino, G.; Triscari, M. Raman and scanning electron microscopy and energy-dispersive X-ray techniques for the characterization of colouring and opaquening agents in Roman mosaic glass tesserae. *J. Raman Spectrosc.* **2004**, *35*, 622–627. [CrossRef]
3. Ricciardi, P.; Colomban, P.; Tournié, A.; Macchiarola, M.; Ayed, N. A non-invasive study of Roman Age mosaic glass tesserae by means of Raman spectroscopy. *J. Archaeol. Sci.* **2009**, *36*, 2551–2559. [CrossRef]
4. Neri, E.; Morvan, C.; Colomban, P.; Guerra, M.F.; Prigent, V. Late Roman and Byzantine mosaic opaque "glass-ceramics" tesserae (5th–9th Century). *Ceram. Int.* **2016**, *42*, 18859–18869. [CrossRef]
5. Neri, E.; Jackson, M.; O'Hea, M.; Gregory, T.; Blet-Lemarquand, M.; Schibille, N. Analyses of glass tesserae from Kilise Tepe: New insights into an early Byzantine production technology. *J. Archaeol. Sci. Rep.* **2017**, *11*, 600–612. [CrossRef]
6. Van der Werf, I.; Mangone, A.; Giannossa, L.C.; Traini, A.; Laviano, R.; Coralini, A.; Sabbatini, L. Archaeometric investigation of Roman tesserae from Herculaneum (Italy) by the combined use of complementary micro-destructive analytical techniques. *J. Archaeol. Sci.* **2009**, *36*, 2625–2634. [CrossRef]
7. Silvestri, A.; Tonietto, S.; Molin, G. The palaeo-Christian glass mosaic of St. Prosdocimus (Padova, Italy): Archaeometric characterisation of "gold" tesserae. *J. Archaeol. Sci.* **2011**, *38*, 3402–3414. [CrossRef]
8. Gliozzo, E.; Santagostino Barbone, A.; Turchiano, M.; Memmi, I.; Volpe, G. The coloured tesserae decorating the vaults of the Faragola balneum (Ascoli Satriano, Foggia, Southern Italy). *Archaeometry* **2012**, *54*, 311–331. [CrossRef]
9. Silvestri, A.; Tonietto, S.; Molin, G.; Guerriero, P. The palaeo-Christian glass mosaic of St. Prosdocimus (Padova, Italy): Archaeometric characterisation of tesserae with antimony- or phosphorus-based opacifiers. *J. Archaeol. Sci.* **2012**, *39*, 2177–2190. [CrossRef]

10. Di Bella, M.; Quartieri, S.; Sabatino, G.; Santalucia, F.; Triscari, M. The glass mosaics tesserae of "Villa del Casale" (Piazza Armerina, Italy): A multi-technique archaeometric study. *Archaeol. Anthropol. Sci.* **2013**, *6*, 345–362. [CrossRef]
11. Silvestri, A.; Tonietto, S.; Molin, G.; Guerriero, P. The palaeo-Christian glass mosaic of St. Prosdocimus (Padova, Italy): Archaeometric characterisation of tesserae with copper- or tin-based opacifiers. *J. Archaeol. Sci.* **2014**, *42*, 51–67. [CrossRef]
12. Paynter, S.; Kearns, T.; Cool, H.; Chenery, S. Roman coloured glass in the Western provinces: The glass cakes and tesserae from West Clacton in England. *J. Archaeol. Sci.* **2015**, *62*, 66–81. [CrossRef]
13. Silvestri, A.; Tonietto, S.; Molin, G.; Guerriero, P. Multi-methodological study of palaeo-Christian glass mosaic tesserae of St. Maria Mater Domini (Vicenza, Italy). *Eur. J. Mineral.* **2015**, *27*, 225–245. [CrossRef]
14. Shortland, A.J. The use and origin of antimonate colorants in early Egyptian glass. *Archaeometry* **2002**, *44*, 517–530. [CrossRef]
15. Freestone, I.C.; Stapleton, C.P.; Rigby, V. The production of red glass and enamel in the Late Iron Age, Roman and Byzantine periods. In *Through a Glass Brightly: Studies in Byzantine and Medieval Art and Archaeology; Presented to David Buckton*; Entwistle, C., Buckton, D., Eds.; Oxbow Books: Oxford, UK, 2003; pp. 142–154, ISBN 978-1785702518.
16. Lahlil, S.; Biron, I.; Galoisy, L.; Morin, G. Technological processes to produce antimonate opacified glass throughout history. In *Proceedings of the Annales du 17e Congrés de l'Association Internationale pour l'Histoire du Verre, Antwerp, Belgium, 4–8 September 2006*; Janssens, K., Degryse, P., Cosyns, P., Caen, J., Van't dack, L., Eds.; University Press Antwerp: Antwerp, Belgium, 2009; pp. 571–578.
17. Molina, G.; Odin, G.P.; Pradell, T.; Shortland, A.J.; Tite, M.S. Production technology and replication of lead antimonate yellow glass from New Kingdom Egypt and the Roman Empire. *J. Archaeol. Sci.* **2014**, *41*, 171–184. [CrossRef]
18. Lahlil, S.; Biron, I.; Galoisy, L.; Morin, G. Rediscovering ancient glass technologies through the examination of opacifier crystals. *Appl. Phys. A* **2008**, *92*, 109–116. [CrossRef]
19. Lahlil, S.; Biron, I.; Cotte, M.; Susini, J. New insight on the in situ crystallization of calcium antimonate opacified glass during the Roman period. *Appl. Phys. A* **2010**, *100*, 683–692. [CrossRef]
20. Lahlil, S.; Cotte, M.; Biron, I.; Szlachetko, J.; Menguy, N.; Susini, J. Synthesizing lead antimonate in ancient and modern opaque glass. *J. Anal. At. Spectrom.* **2011**, *26*, 1040–1050. [CrossRef]
21. Brill, R.H.; Cahill, N.D. A red opaque glass from Sardis and some thoughts on red opaques in general. *J. Glass Stud.* **1988**, *30*, 16–27.
22. Barber, D.J.; Freestone, I.C.; Moulding, K.M. Ancient copper red glasses: Investigation and analysis by microbeam techniques. In *From Mine to Microscope. Advances in the Study of Ancient Technology*; Shortland, A.J., Freestone, I.C., Rehren, T., Eds.; Oxbow Books: Oxford, UK, 2009; pp. 115–127, ISBN 978-1-84217-259-9.
23. Schibille, N.; McKenzie, J. Glass tesserae from Hagios Polyeuktos, Constantinopole: Their early Byzantine affiliations. In *Neighbours and Successors of Rome. Tradition of Glass Production and Use in Europe and the Middle East in the Later 1st Millenium AD*; Keller, D., Price, J., Jackson, C.M., Eds.; Oxbow Books: Oxford, UK, 2014; pp. 114–127, ISBN 978178297397.
24. Verità, M. Analisi di tessere musive vitree del battistero della Basilica di San Marco in Venezia. In *Proceedings of the Scienza e Tecnica del Restauro della Basilica di San Marco: Atti del Convegno Internazionale di Studi, Venezia, Italy, 16–19 May 1995*; Vio, E., Lepschy, A., Eds.; Istituto Veneto di Scienze, Lettere ed Arti: Venezia, Italy, 1999; pp. 567–585, ISBN 8886166796.
25. Tite, M.S.; Shortland, A.J. Production technology for copper-and cobalt-blue vitreous materials from the New Kingdom site of Amarna—A reappraisal. *Archaeometry* **2003**, *45*, 285–312. [CrossRef]
26. Vichy, M.; Picon, M.; Thirion-Merle, V. Le manganèse comme impureté, décolorant ou colorant des verres au natron. *Bull. l'AFAV* **2002**, 15–17. Available online: http://www.afaverre.fr/pdf/bull2002/07_Bull2002_M._Vichy%20et%20alii_p15-17.pdf (accessed on 15 June 2018).
27. Barca, D.; Basso, E.; Bersani, D.; Galli, G.; Invernizzi, C.; La Russa, M.F.; Lottici, P.P.; Malagodi, M.; Ruffolo, S.A. Vitreous tesserae from the calidarium mosaics of the Villa dei Quintili, Rome. Chemical composition and production technology. *Microchem. J.* **2016**, *124*, 726–735. [CrossRef]
28. Conte, A.; Salvadori, M.; Tirone, C. *La Villa Romana di Torre di Pordenone. Tracce della Residenza di un Ricco Dominus Nella Cisalpina Orientale*; Quasar: Roma, Italy, 1999; ISBN 8871401654.

29. Guaitoli, M.T. Il progetto di Santa Maria Maggiore (Trento). Relazione preliminare: Dallo scavo alla diffusione dei dati. *J. Fasti Online* **2011**, *238*, 1–18.
30. Maltoni, S.; Silvestri, A. Innovation and tradition in the fourth century mosaic of the Casa delle Bestie Ferite in Aquileia, Italy: Archaeometric characterisation of the glass tesserae. *Archaeol. Anthropol. Sci.* **2018**, *10*, 415–429. [CrossRef]
31. Brill, R.H. *Chemical Analyses of Early Glasses. Volume 2 Tables of Analyses*; The Corning Museum of Glass: Corning, NY, USA, 1999; ISBN 0-872900-143-2.
32. Savitzky, A.; Golay, M.J.E. Smoothing and differentiation of data by simplified least squares procedures. *Anal. Chem.* **1964**, *36*, 1627–1639. [CrossRef]
33. Lilyquist, C.; Brill, R.H. *Studies in Early Egyptian Glass*; Metropolitan Museum of Art: New York, NY, USA, 1993; ISBN 978-0300200195.
34. Jackson, C.M.; Cottam, S. "A green thought in a green shade"; Compositional and typological observations concerning the production of emerald green glass vessels in the 1st century A.D. *J. Archaeol. Sci.* **2015**, *61*, 139–148. [CrossRef]
35. Van Der Linden, V.; Cosyns, P.; Schalm, O.; Cagno, S.; Nys, K.; Janssens, K.; Nowak, A.; Wagner, B.; Bulska, E. Deeply Coloured and black glass in the northern provinces of the Roman empire: Differences and similarities in chemical composition before and after AD 150. *Archaeometry* **2009**, *51*, 822–844. [CrossRef]
36. Maltoni, S.; Silvestri, A.; Molin, G. Opaque red glass tesserae from Roman and early-Byzantine sites of north-eastern Italy: New light on production technologies. In *Proceedings of the Annales du 20e Congrès de l'Association Internationale pour l'Histoire du Verre, Fribourg, Switzerland, 7–11 September 2015*; Wolf, S., de Pury-Gysel, A., Eds.; Verlag Marie Leidorf GmbH: Rahden, Germany, 2017; pp. 280–287.
37. Jackson, C.M.; Paynter, S. A Great Big Melting Pot: Exploring Patterns of Glass Supply, Consumption and Recycling in Roman Coppergate, York. *Archaeometry* **2015**, *58*, 68–95. [CrossRef]
38. Schibille, N.; Sterrett-Krause, A.; Freestone, I.C. Glass groups, glass supply and recycling in late Roman Carthage. *Archaeol. Anthropol. Sci.* **2017**, *9*, 1223–1241. [CrossRef]
39. Silvestri, A.; Gallo, F.; Maltoni, S.; Degryse, P.; Ganio, M.; Longinelli, A.; Molin, G. Things that travelled—A review of the Roman glass from Northern Adriatic Italy. In *Things That Travelled: Mediterranean Glass in the First Millennium CE*; Daniela Rosenow, D., Phelps, M., Meek, A., Freestone, I.C., Eds.; UCL Press: London, UK, 2018; pp. 346–367, ISBN 978-1-78735-117-2.
40. Silvestri, A. The coloured glass of Iulia Felix. *J. Archaeol. Sci.* **2008**, *35*, 1489–1501. [CrossRef]
41. Silvestri, A.; Molin, G.; Salviulo, G. The colourless glass of Iulia Felix. *J. Archaeol. Sci.* **2008**, *35*, 331–341. [CrossRef]
42. Gallo, F.; Silvestri, A.; Molin, G. Glass from the Archaeological Museum of Adria (North–East Italy): New insights into Early Roman production technologies. *J. Archaeol. Sci.* **2013**, *40*, 2589–2605. [CrossRef]
43. Maltoni, S.; Silvestri, A.; Marcante, A.; Molin, G. The transition from Roman to Late Antique glass: New insights from the Domus of Tito Macro in Aquileia (Italy). *J. Archaeol. Sci.* **2016**, *73*, 1–16. [CrossRef]
44. Neri, E.; Verità, M. Glass and metal analyses of gold leaf tesserae from 1st to 9th century mosaics. A contribution to technological and chronological knowledge. *J. Archaeol. Sci.* **2013**, *40*, 4596–4606. [CrossRef]
45. Verità, M.; Zecchin, S. Scientific investigation of Byzantine glass tesserae from the mosaics on the south chapel of Torcello's Basilica, Venice. In *Proceedings of the Annales du 18e Congrès de l'Association International pour l'Histoire du Verre, Thessaloniki, Greece, 20–25 September 2009*; Ignatiadou, D., Antonaras, A., Eds.; ZITI Publishing: Thessaloniki, Greece, 2012; pp. 315–320.
46. Gedzevičiūtė, V.; Welter, N.; Schüssler, U.; Weiss, C. Chemical composition and colouring agents of Roman mosaic and millefiori glass, studied by electron microprobe analysis and Raman microspectroscopy. *Archaeol. Anthropol. Sci.* **2009**, *1*, 15–29. [CrossRef]
47. Basso, E.; Invernizzi, C.; Malagodi, M.; La Russa, M.F.; Bersani, D.; Lottici, P.P. Characterization of colorants and opacifiers in roman glass mosaic tesserae through spectroscopic and spectrometric techniques. *J. Raman Spectrosc.* **2014**, *45*, 238–245. [CrossRef]
48. Lahlil, S.; Biron, I.; Cotte, M.; Susini, J.; Menguy, N. Synthesis of calcium antimonate nano-crystals by the 18th dynasty Egyptian glassmakers. *Appl. Phys. A* **2010**, *98*, 1–8. [CrossRef]
49. Mass, J.L.; Stone, R.E.; Wypyski, M.T. The mineralogical and metallurgical origins of Roman opaque colored glasses. In *Prehistory and History of Glassmaking Technology*; McCray, P., Kingery, D.W., Eds.; American Ceramic Society: Columbus, OH, USA, 1998; pp. 121–145, ISBN 9781574980417.

50. Gratuze, B.; Soulier, I.; Barrandon, J.N.; Foy, D. De l'origine du cobalt dans les verres. *Rev. d'Archéométrie* **1992**, *16*, 97–108. [CrossRef]
51. Henderson, J. *The Science and Archaeology of Materials: An Investigation of Inorganic Materials*; Routledge: London, UK, 2000; ISBN 0415199336.
52. Bamford, C.R. *Colour Generation and Control in Glass*; Elsevier Scientific Publishing Company: Amsterdam, The Netherlands, 1977; Volume 3, ISBN 1520-6378.
53. Cascales, C.; Alonso, J.A.; Rasines, I. NEW PYROCHLORES Pb2(MSb) O 6.5 (M equals Ti,Zr,Sn,Hf). *J. Mater. Sci. Lett.* **1986**, *5*, 675–677. [CrossRef]
54. Rosi, F.; Manuali, V.; Miliani, C.; Brunetti, B.G.; Sgamellotti, A.; Grygar, T.; Hradil, D. Raman scattering features of lead pyroantimonate compounds. Part I: XRD and Raman characterization of Pb2Sb2O7 doped with tin and zinc. *J. Raman Spectrosc.* **2009**, *40*, 107–111. [CrossRef]
55. Rosi, F.; Manuali, V.; Grygar, T.; Bezdicka, P.; Brunetti, B.G.; Sgamellotti, A.; Burgio, L.; Seccaroni, C.; Miliani, C. Raman scattering features of lead pyroantimonate compounds: Implication for the non-invasive identification of yellow pigments on ancient ceramics. Part II. In situ characterisation of Renaissance plates by portable micro-Raman and XRF studies. *J. Raman Spectrosc.* **2011**, *42*, 407–414. [CrossRef]
56. Wypyski, M.T.; Becker, L. Glassmaking Technology at Antioch. In *The Arts of Antioch: Art Historical and Scientific Approaches to Roman Mosaics and a Catalogue of the Worchester Art Museum Antioch Collection*; Becker, L., Kondoleon, C., Eds.; Princeton University Press: Princeton, NJ, USA, 2005; pp. 115–175, ISBN 9780691122328.
57. Verità, M.; Maggetti, M.; Saguì, L.; Santopadre, P. Colors of Roman glass: An investigation of the yellow sectilia in the Gorga collection. *J. Glass Stud.* **2013**, *55*, 39–52.
58. Sandalinas, C.; Ruiz-Moreno, S. Lead-Tin-Antimony Yellow: Historical Manufacture, Molecular Characterization and Identification in Seventeenth-Century Italian Paintings. *Stud. Conserv.* **2004**, *49*, 41–52. [CrossRef]
59. Hradil, D.; Grygar, T.; Hradilová, J.; Bezdicka, P.; Grunwaldová, V.; Fogaš, I.; Miliani, C. Microanalytical identification of Pb-Sb-Sn yellow pigment in historical European paintings and its differentiation from lead tin and Naples yellows. *J. Cult. Herit.* **2007**, *8*, 377–386. [CrossRef]
60. Freestone, I.C. Chemical analysis of raw glass fragments. In *Excavation at Carthage, The Circular Harbour, North Side. The Site and Finds Other than Pottery*; British Academy Monographs in Archeology; Hurst, H.R., Ed.; Oxford University Press: Oxford, UK, 1994; Volume 2, p. 290, ISBN 0-19-727003-4 hbk.
61. Paynter, S.; Kearns, T. *West Clacton Reservoir, Great Bentley, Essex. Analysis of Glass Tesserae*; Technology Report; English Heritage: Portsmouth, UK, 2011; Volume 44.
62. Jackson, C.M.; Cottam, S.; Lazar, I. The green, green glass of Rome. In *Proceedings of the Annales du 19e Congrès de l'Association International pour l'Histoire du Verre, Piran, Slovenia, 17–21 September 2012*; Lazar, I., Ed.; AIHV: Thessaloniki, Greece, 2015; pp. 109–117.
63. Schibille, N.; Degryse, P.; Corremans, M.; Specht, C.G. Chemical characterisation of glass mosaic tesserae from sixth-century Sagalassos (south–west Turkey): Chronology and production techniques. *J. Archaeol. Sci.* **2012**, *39*, 1480–1492. [CrossRef]
64. Rehren, T.; Pusch, E.B. Late Bronze Age glass production at Qantir-Piramesses, Egypt. *Science* **2005**, *308*, 1756–1758. [CrossRef] [PubMed]
65. Cable, M.; Smedley, J.W. The replication of an opaque red glass from Nimrud. In *Early Vitreous Materials*; British Museum Occasional Paper 56; Bimson, M., Freestone, I.C., Eds.; British Museum: London, UK, 1987; pp. 151–164, ISBN 978-0861590568.
66. Ahmed, A.A.; Ashour, G.M. Effect of heat treatment on the crystallisation of cuprous oxide in glass. *Glass Technol.* **1981**, *22*, 24–33.
67. Freestone, I.C. Composition and microstructure of early opaque red glass. In *Early Vitreous Material*; British Museum Occasional Paper 56; Bimson, M., Freestone, I.C., Eds.; British Museum: London, UK, 1987; pp. 173–191, ISBN 9780861590568.
68. Stapleton, C.P.; Freestone, I.C.; Bowman, S.G.E. Composition and origin of Early Mediaeval opaque red enamel from Britain and Ireland. *J. Archaeol. Sci.* **1999**, *26*, 913–921. [CrossRef]